

IN-34-CR  
157065  
P-38



**FLORIDA ATLANTIC UNIVERSITY**  
College of Engineering • Department of Ocean Engineering  
**Center for Acoustics and Vibrations**



(NASA-CR-183165) POWER FLOW ANALYSIS OF TWO  
COUPLED PLATES WITH ARBITRARY  
CHARACTERISTICS Semiannual Report No. 4  
(Florida Atlantic Univ.) 38 p CSCI 20D

N88-28251

Unclas  
G3/34 0157065

POWER FLOW ANALYSIS  
OF TWO COUPLED PLATES WITH  
ARBITRARY CHARACTERISTICS

J. M. Cuschieri  
Center for Acoustics and Vibration  
Department of Ocean Engineering  
Florida Atlantic University  
Boca Raton, Florida 33431

August, 1988

Fourth Semi-annual Report  
Grant Number NAG-1-685

Submitted to

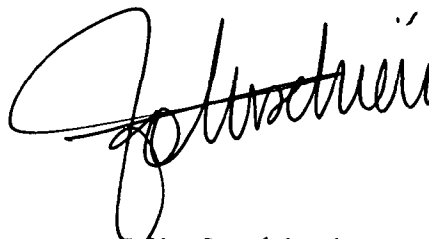
National Aeronautics and Space Administration  
Langley Research Center  
Hampton, VA 23665

## FORWARD

This report describes the work performed during the second-half of the second year of the research project sponsored by NASA Langley Research Center under Research Contract NAG-1-685, entitled "Use of Energy Accountancy and Power Flow Techniques for Aircraft Noise Transmission". The author would like to acknowledge the financial support by NASA Langley through the Acoustics Division. Also special thanks to the graduate assistants who worked on this project and to the department of Ocean Engineering at Florida Atlantic University.

During this second half of the second year, two Masters' thesis were completed with titles, "Power Flow Analysis of Simple Structures" and "Transmission of Vibrational Power in Joined Structures" The abstracts of these two Master thesis have been submitted for publication in the Journal of the Acoustical Society of America in the Technical Notes and Research Briefs Section.

Submitted by

A handwritten signature in black ink, appearing to read "J.M. Cuschieri". The signature is written in a cursive style with a large initial "J" and a long horizontal stroke.

J.M. Cuschieri

Principal Investigator

## ABSTRACT

In the last progress report (February, 88) some results were presented for a parametric analysis on the vibrational power flow between two coupled plate structures using the mobility power flow approach, where the vibrational power transfer and power input are expressed in terms of mobility functions. The results reported then are for changes in the structural parameters of the two plates, but with the two plates, identical in their structural characteristics. In this report, the limitation of keeping the two plates identical is removed and the vibrational power input and output are evaluated for different area ratios, plate thickness ratios and for different values of the structural damping loss factor for the source plate (plate with excitation) and the receiver plate. In performing this parametric analysis, the source plate characteristics are kept constant. The purpose of this parametric analysis is to be able to determine the most critical parameters that influence the flow of vibrational power from the source plate to the receiver plate. In the case of the structural damping parametric analysis, the influence of changes in the source plate damping is also investigated. As was done in the previous (February, 1988), progress report the results obtained from the mobility power flow approach will be compared to results obtained using a Statistical Energy Analysis (SEA) approach, some of these SEA results have been reported in the February, 1988 progress report. The significance of the power flow results are discussed together with a discussion and a comparison between the SEA results and the mobility power flow results. Furthermore, the benefits that can be derived from using the mobility power flow approach, are also examined.

## INTRODUCTION

In previous work dealing with the use of the mobility power flow approach for the analysis of two coupled plate structures joined along a line junction [1,2], treated the extension of this technique to line connections. This represents an improvement on earlier work on the mobility power flow method [3,4] where only point contacts, hence mobility functions defined for single point location, were used. While the first work defined the mobility power flow approach and its advantages when used for structural dynamic analysis, and the more recent work extends the technique to the two dimensional case, in this latter work a restriction was imposed on the type of analysis that can be performed, namely that the two plate structures used in the analysis must be identical. Thus some generalizations were required to allow for the analysis of coupled plate structures when the two plates are not identical. This issue of generalization is what is being addressed in this report. As anticipated, generalizing the expressions used in the approach, so that plates with different structural characteristics can be investigated increased the complexity of the expressions and also the required computation time. However, the advantages of the mobility power flow technique over other methods of analysis in the mid-frequency range still hold.

With this generalization, the mobility functions at the joint are completely defined, that is line mobilities have been obtained as a modal sum with a weighting function based on the location of the excitation. Therefore any combination of plate structures can now be considered. Additionally, what has been derived for the L-shaped plate holds equally well for two plates joined along a common boundary, in a flat configuration, with a rigid line stiffener all along the joint between the two plates. Thus, two alternate uses can be made of this mobility power flow approach. One alternative would be as a parametric analysis, similar to what is being presented in this report, to optimize the parameters that control the flow of vibrational power between the source plate and the receiver plate. In this case, the influence of a flexible stiffener can also be investigated by introducing additional mobility functions at the joint. The second alternative would be to consider the problem of multiple connected plate structures forming a periodic or quasi periodic structure. Although this may require more of an effort to formulate the problem, the approach is similar to that of two connected structures with the exception that all the power flow equations would be written in matrix form. For perfectly periodic structures, the mobility power flow approach would be very efficient since the mobility functions for each subelement of the periodic structure need only be evaluated once for just one of the spans. In the periodic structure analysis, it would be useful to transform the analysis from the space domain to the wavenumber domain in the direction along the joints to simplify the representation. With this transform, the analysis

becomes identical to that of a one dimensional periodic structure with point junctions except that an inverse transform back to the space domain would be required on the final results.

The issues mentioned in the above paragraph are the topic of this progress report and thus it consists of two sections. The next section deals with the generalization of previous power flow results [2] to deal with plates of different structural characteristics including a parametric analysis. Results are presented for plates with four different area ratios, five different thickness ratios and six conditions of different structural damping. These results are later on compared to SEA results. In the following section, the development of the mobility power flow approach for the case of multiple connected structures is presented. Since, if a transform is used, the same type of analysis applies to point or line joints, the formulation and results of this section are restricted to periodic beams with different number of spans and different characteristics for the stiffeners defining the spans.

#### MOBILITY POWER FLOW

In the development of the power flow expression for two coupled plates (figure 1) - equations (14) and (15) in [2] - it was assumed that the coupled plates are identical. This led to the simplification in evaluating the transferred vibrational power  $P_{trans}$  that

$$\dot{\theta}_3 = \frac{-M_3}{M_2 + M_3} \dot{\theta}_F = -\frac{\dot{\theta}_F}{2} \quad (1)$$

where  $M_2$  and  $M_3$  are the line mobilities at the joint for the source plate and the receive plate respectively,  $\dot{\theta}_F$  is the angular velocity at the junction of the source plate due to the application of the excitation when the source plate is uncoupled from the receiver plate and  $\dot{\theta}_3$  is the angular velocity at the junction of the receiver plate when coupled to the source plate. The simplification in equation (1) comes about since, for identical plates,  $M_2 = M_3$ . Furthermore, as a consequence of this result (equation 1) the evaluation of the integral for the transferred power over the entire length of the junction,

$$P_{trans} = \frac{1}{2} \int_0^a \text{Real} \left\{ T^*(x) \dot{\theta}_3(x) \right\} dx \quad (2)$$

can be evaluated analytically. The two summations for  $T_{n_1}(x)$  and  $\theta_3(x)$

$$\sum_{n_1=1}^{\infty} T_{n_1}^* \sin\left(\frac{n_1 \pi x}{a}\right) \quad (3)$$

$$\sum_{n_1=1}^{\infty} \theta_{F n_1} \sin\left(\frac{n_1 \pi x}{a}\right) \quad (4)$$

when multiplied and integrated over  $x$ , due to orthogonality, reduce to a single summation over  $n_1$ .

For plates with different structural characteristics, equation (1) does not hold and thus the integration cannot any more be done analytically. This also means that  $M_2$  and  $M_3$  must be completely defined. Starting first with obtaining an expression for the moment distribution along the junction, from equations (A.14), (A.16) and (A.17) in reference [2], the moment distribution, normalized with respect to the applied excitation force  $F$  is given by

$$\frac{T(x)}{F} = \frac{4f}{a b_1^2} \sqrt{\frac{D_1}{\rho_1 h_1}} \sum_{n_1, n_2}^{\infty} \frac{(-1)^{n_2} n_2 \sin\left(\frac{n_1 \pi x_0}{a}\right) \sin\left(\frac{n_2 \pi y_0}{b_1}\right) \sin\left(\frac{n_1 \pi x}{a}\right)}{[(f_n^*)^2 - f^2] [A + R B]}$$

where

$$A = k_1 \coth(k_1 b_1) - k_2 \cotg(k_2 b_1)$$

$$B = k'_1 \coth(k'_1 b_2) - k'_2 \cotg(k'_2 b_2)$$

$$R = \left[ \left( \rho_1 h_1 D_1^* \right) / \left( \rho_2 h_2 D_2^* \right) \right]^{1/2}$$

(5 a, b, c, d)

The notation used is the same as that in [2], that is  $f$  is the frequency,  $\rho_i$ ,  $h_i$ ,  $b_i$ ,  $D_i^*$  are respectively the density, thickness, length and flexural rigidity of plate  $i$ ,  $i = 1$  or  $2$ ,  $a$  is the width of the plates and the junction,  $f_n^*$  is the  $n$ th modal frequency, and  $k_1$  and  $k_2$  are defined by

$$\begin{aligned} k_1^2 &= 2 k_x^2 + k_y^2 \\ k_2^2 &= k_y^2 \end{aligned} \quad (6a,b)$$

where  $k_x$  and  $k_y$  are the wavenumbers in the  $x$  and  $y$  directions respectively. The wavenumbers with a prime in the expression for  $B$  above indicate that these pertain to the receiver plate, plate 2, while without the prime are for the source plate, plate 1.

An important feature to notice with regards to the moment expression (Equation 5) is that while the moment can be expressed as a sum of contributions of sinusoidal terms, which come about because of the way in which the plate would deflect in rotation under uncoupled conditions, the terms are weighted by a set of sine functions the values of which are controlled by the values of  $x_0$  and  $y_0$ . That is the amplitude of the moment components are determined by the mode of vibration of the source plate, controlled by the location of the excitation force.

Using Equation (5) for the moment distribution and substituting in equation (A.12) of reference [2], two expressions for the edge mobilities are obtained. The expressions for  $M_2$  and  $M_3$  defined as the ratio of angular rotation per unit applied moment are not similar with only a change of subscript from 1 to 2, and the reason for this is that the influence of the moment distribution is the same in both cases. Thus



$$M_2(x) = \frac{-j}{2\sqrt{\rho_1} h_1 D_1^*} \frac{\sum_{n_1, n_2} \left\{ \frac{(-1)^{n_2} n_2 \sin\left(\frac{n_1 \pi x_0}{a}\right) \sin\left(\frac{n_2 \pi y_0}{b_1}\right) \sin\left(\frac{n_1 \pi x}{a}\right)}{\left[ (f_n^*)^2 - f^2 \right] \left[ 1 + R B / A \right]} \right\}}{\sum_{n_1, n_2} \left\{ \frac{(-1)^{n_2} n_2 \sin\left(\frac{n_1 \pi x_0}{a}\right) \sin\left(\frac{n_2 \pi y_0}{b_1}\right) \sin\left(\frac{n_1 \pi x}{a}\right)}{\left[ (f_n^*)^2 - f^2 \right] \left[ A + R B \right]} \right\}} \quad (6)$$

and

$$M_3(x) = \frac{-j}{2\sqrt{\rho_2} h_2 D_2^*} \frac{\sum_{n_1, n_2} \left\{ \frac{(-1)^{n_2} n_2 \sin\left(\frac{n_1 \pi x_0}{a}\right) \sin\left(\frac{n_2 \pi y_0}{b_1}\right) \sin\left(\frac{n_1 \pi x}{a}\right)}{\left[ (f_n^*)^2 - f^2 \right] \left[ R + A / B \right]} \right\}}{\sum_{n_1, n_2} \left\{ \frac{(-1)^{n_2} n_2 \sin\left(\frac{n_1 \pi x_0}{a}\right) \sin\left(\frac{n_2 \pi y_0}{b_1}\right) \sin\left(\frac{n_1 \pi x}{a}\right)}{\left[ (f_n^*)^2 - f^2 \right] \left[ A + R B \right]} \right\}} \quad (7)$$

Where A, B and R have the same definitions as in equation (5), and the same notation is used.

By combining these three equations (5), (6) and (7) together with equations from [2] into the power flow expressions, namely

$$\frac{P_{in}}{|F(f)|^2} = \frac{1}{2} \text{Real} \left\{ M_1 - \frac{M_{12} M_{21}}{M_2 + M_3} \right\} \quad (8)$$

and

$$\frac{P_{\text{trans}}}{|F(f)|^2} = \frac{1}{2} \left| \frac{M_{12}}{M_2 + M_3} \right|^2 \text{Real} \left\{ M_3 \right\} \quad (9)$$

and integrating this last expression over the length of the joint, the input and transmitted power can be evaluated for the case of two plates joined along a common edge, which is pinned, but with the plates having different structural characteristics. By using equations (5), (6) and (7) as they show in this report, the influence of plate areas, thickness, damping and materials on the input and transmitted power can be investigated. The results of this parametric analysis and the comparison of results with parametric analysis results using SEA are presented in the next section.

### 3. PARAMETRIC ANALYSIS RESULTS

The results presented in [1] using an SEA approach investigate changes in the power ratio, defined as the ratio of the power transmitted to the input power, with changes in the area ratio, thickness ratio, damping ratio, and changes in the material type of the plates. The same parameters will be investigated here and results will be presented for the following conditions.

- (a) Area ratios (defined as ratio of receiver plate area to source plate area): 0.25; 0.5; 1.0; 2.0.
- (b) Thickness ratios (ratio of receiver plate thickness to source plate thickness) : 0.125; 0.25; 0.5; 1.0; 2.0; 4.0.
- (c) Damping (receiver plate damping loss factor source plate damping loss factor) : 0.1/ 0.001; 0.01 / 0.001 ; 0.1 / 0.01 ; 0.001/ 0.01; 0.01 / 0.1 ; 0.001 / 0.1.
- (d) Material types (receiver plate material/ source plate material): Aluminum / Aluminum, Steel / Aluminum.

Together with the results obtained using the mobility power flow approach, the results from [1] using SEA are also presented for comparison. In all of the analysis, except where indicated, the following base conditions for the source plate are considered.

Density = 2710 kg/m <sup>3</sup> ;	Thickness = 0.00635m ;
length = 0.5m ;	Width = 1.0 m ;
Poisson ratio = 0.33 ;	Loss factor = 0.01 ;
Young's Modulus = 7.2E+10 N/m <sup>2</sup> .	

### 3.1 Influence of Area Variations

The results for changes in the ratio of the area of the two plates are shown in figures (2) and (3). The first observation that can be made regarding these results is that as expected, as the area of the receiver plate increases, the number of modes of the coupled system increases (figure 2(a)). While as the area of the receiver plate decreases the number of modes decrease (figure 2(b)). Figure (4) is a reproduction of the results for the power ratio using an SEA approach which were presented in reference [1]. Comparing the results in figure (3) with the results in figure (4), there is in general a very good agreement between the two sets of results, in the sense that as the area ratio increases, the general level of the power ratio also increases. However, the exact value of the power ratio is very much dependent on the frequency. That is while the general level may decrease as the area ratio decreases, for those modes that can be associated with the receiver plate, a significant portion of the input power finds its way into the receiver plate. From figures (2(c)) and (3(c)) it can be observed that for the two modes one just under  $400 \text{ Hz}$  and one at approximately  $700 \text{ Hz}$ , roughly equipartition of vibrational power exists between the source and the receiver plates.

### 3.2. Influence of Thickness Variations

The variations in the power flow results with changes in the thickness ratio are shown in figures (5) and (6). In general similar results are obtained in this case to those for changes in the plate areas except that in this case a peak in the general level of the power ratio is obtained in the region where the thickness ratio is close to unity. As the thickness ratio decreases, the number of modes of the receiver plate increase and thus there is an increase in the number of modes of the coupled system, while the general level of the power ratio decreases. These general results are similar to those obtained using an SEA approach (figure 7). However, at those frequencies which correspond to modes of the receiver plate, a significant amount of vibrational power can again be transferred between the source plate and the receiver plate. This is very well demonstrated in figure (6(f)), where while the general level is low, there are peaks in the power ratio curve corresponding to the modes which can be attributed to the receiver plate.

As pointed out earlier in this subsection, the variations in the power ratio with changes in thickness differ from the variations associated with changes in area in that the power ratio decreases as the thickness ratio increases. Apart from this decrease in the power ratio, the number of modes also decrease (figure 5(a)). However, in this case as well, for those modes which belong to the receiver plate, the power ratio can be significant and if the receiver mode happens to be at a trough in the behavior of the source plate, almost all the vibrational power supplied to the source plate is transferred to the receiver plate. Figure (6 (a)) is

a good representation of this in that while the general level is low, there are two peaks in the power ratio curve where the transferred power is more than 50% of the input power. This type of result shows the significance of using the mobility power flow method over other methods such as SEA, where the averaged results can be misleading at particular frequencies.

### 3.3 Influence of Damping

The damping loss factor values that are selected for the analysis are similar to those used in the SEA results presented in [1]. Figure (8) represents the power input and power transfer curves and figure (9) shows the power ratio curves for the different damping loss factor values. In this case, there are no changes in the number of modes of the coupled system since the size and thickness of both plates remain constant. However, the curves exhibit some smoothing of the modes as the damping loss factor increases. An interesting point is that the smoothing of the power input and transferred curves occurs irrespective of whether the damping increases in the source plate or the receiver plate.

Comparing the results to the SEA results (figure 10), again there is good general agreement between the two sets of results. However, similar to the other parametric changes, significant fluctuations exist between the mean (SEA) results and the actual results. Contrary to what would be expected, the fluctuations between the mean results and the actual results for the power ratio do not always decrease with increases in the damping of any of the two plates. This again shows the importance of analysis techniques which do not produce averaged results since at any one frequency, the fluctuations from the mean averaged values can be significant. These fluctuations cannot be assumed to decrease in amplitude by increases in the structural damping of the components of the structure, that is by increasing the interaction between the modes.

With regards to the meaning of the results, the power ratio exhibits values close to unity when the damping of the receiver plate is high compared to the damping of the source plate. Most of the input power flows to the receiver plate structure. As the damping of the source plate increases less vibrational power flows into the receiver plate. In the case where the source plate damping is much higher than the receiver plate damping, the value of the power ratio is extremely low implying that only a small portion of the input power is transferred to the receiver plate. However at particular frequencies, such as at resonances of the receiver structure, the power ratio can still reach values higher than the general mean low level (figure 9(f)).

### 3.4 Influence of Structure Material

A set of results are obtained for changes in the material of one of the plate substructures. One other type of material is considered, and the reason for this is to be consistent with the SEA results in [1] and thus be able to compare the results from the two techniques. Figures (11) and (12) show the results for the power input and output and the power ratio obtained using the mobility power flow technique, together with the results from SEA, for the case when the source plate substructure material is changed from aluminum to steel. Comparing these two sets of results, the mobility power flow predictions show that the general level for the power ratio remains approximately the same as that for the case when both plate substructures are of the same material. This is consistent with the SEA results. However, the exact detailed characteristics of the power ratio curve are different for the case of different substructure materials (figures 11(b)) as compared to the case of the same material (figure 3(b)). This is consistent with all the results that have been presented thus far using the mobility power flow approach.

The above results for changes in areas, thicknesses, damping and material demonstrate a typical parametric analysis for two coupled structures using the mobility power flow approach. In performing the analysis, while the evaluation of the mobility functions was very time consuming, these evaluations were not required to be repeated for each change in the parameters of the global structure. Only those mobility functions which were effected by changes in the parameters of the substructures had to be re-evaluated. That is the mobility functions of the particular substructure for which parametric changes are considered. This made the analysis very efficient since, if the only parametric changes made are for the receiver plate, then only  $M_3$  had to be re-evaluated, while the remaining mobility functions were obtained from data files stored from previous evaluations of these functions. This is what makes the mobility power flow method a very attractive tool for structural analysis.

### 4. EXTENSION TO MULTIPLE CONNECTED STRUCTURES

In extending the mobility power flow technique to line connected structures, it has been shown that the fundamental expressions for the vibrational power input and output are not different from those for point connected structures, except that the mobility functions are space variables as well as frequency variables, and for the transferred vibrational power the expression for the power is integrated over the entire length of the joint. Thus in extending the mobility power flow method to multiple connected structures, one only needs to formulate the approach to one dimensional structures. The application to two dimensional functions then just follows the same extensions as for the example of the two coupled plate structures that have been presented thus far.

Additionally, the results that have been obtained for the L-shaped beam [3] and the L-shaped plate hold equally well for two coupled plate or beam structures in a side by side configuration as shown in figure (13). That is, with an extension of this analysis to multiple coupled structures, this mobility power flow approach can be used to deal with periodic structures. The application of this mobility power flow technique to a periodic beam configuration with both rigid and flexible supports between the spans will be discussed in this section. In the case of flexible supports the formulation also shows how mobility elements can be introduced at the joints between the substructures to model such elements as stiffeners and dissipative junctions.

#### 4.1 Basic Approach

Considering first a series of linearly coupled structures, (figure 14) where  $V_i$  ( $i = A, B, C$ , etc) represent the motion of the junctions which may be rotational or translational and  $F_i$  ( $i = A, B, C$ , etc) represent forces or moments that are transmitted across the junction. Since in all the previous analysis the power flow method has been restricted to point loading, it is assumed here that the coupled structure is excited by a point load on one of the substructures. Writing down the relationships for the velocities and the loads for each of the junctions of the multiple coupled structure:

$$\begin{aligned}
 V_1 &= F_1 M_1 + F_A M_{12} \\
 V_A &= F_1 M_{21} + F_A M_2 = -F_A M_3 - F_B M_{34} \\
 V_B &= -F_A M_{43} - F_B M_4 = F_B M_5 + F_C M_{56} \\
 &\text{etc.}
 \end{aligned}
 \tag{10}$$

where  $F_1$  is the input loading and  $M_i$  and  $M_{ik}$  represent respectively the input mobility functions and transfer mobility functions.

In the derivation of the equations for the solution of this multiple coupled structure, the number of substructures is limited to four. Also, instead of writing complete expressions for the input and transferred power between the substructures, the relationships are written in matrix form, which allow for the expansion of the solution to more than four substructures by adding terms in the matrices in the same pattern as those identified with just four substructures. Thus, the matrix relationships for the velocities and forces for the four coupled substructures case are as follows:

$$\begin{bmatrix} (M_2 + M_3) & -M_{34} & 0 \\ -M_{43} & (M_4 + M_5) & -M_{56} \\ 0 & -M_{65} & (M_6 + M_7) \end{bmatrix} \begin{bmatrix} F_A \\ F_B \\ F_C \end{bmatrix} = \begin{bmatrix} M_{21} & F_1 \\ 0 \\ 0 \end{bmatrix} \quad (11)$$

$$\begin{bmatrix} V_1 \\ V_A \\ V_B \\ V_C \end{bmatrix} = \begin{bmatrix} M_1 & -M_{12} & 0 & 0 \\ 0 & M_3 & -M_{34} & 0 \\ 0 & 0 & M_5 & -M_{56} \\ 0 & 0 & 0 & M_7 \end{bmatrix} \begin{bmatrix} F_1 \\ F_A \\ F_B \\ F_C \end{bmatrix} \quad (12)$$

and the power flows are given by

$$\begin{bmatrix} P_1 \\ P_A \\ P_B \\ P_C \end{bmatrix} = \text{Real} \left\{ \begin{bmatrix} V_1^* & 0 & 0 & 0 \\ 0 & V_A^* & 0 & 0 \\ 0 & 0 & V_B^* & 0 \\ 0 & 0 & 0 & V_C^* \end{bmatrix} \begin{bmatrix} F_1 \\ F_A \\ F_B \\ F_C \end{bmatrix} \right\} \quad (13)$$

where  $P_1$  represents the power input and  $P_A$ ,  $P_B$ , etc represent the power flow between the spans at junctions  $A$ ,  $B$ , etc. respectively. The procedure for the solution would be to first evaluate the junction loadings,  $F_A$ ,  $F_B$ , etc, from equation (11) and use these values in equation (12) to solve for the velocities. Having obtained the velocities and the loadings at the junctions the power flow is evaluated using equation (13).

Applying the above approach to a periodic beam with rigid supports between the spans, with a transverse point load applied at the midpoint of the first span. The loadings  $F_A$ ,  $F_B$ , etc., in this case would represent moments applied at the junctions and the velocities  $V_A$ ,  $V_B$ , etc. would represent rotational velocities. The results for different number of spans are shown in figure (15). As would be expected, the introduction of the additional spans would create additional resonant modes. As the number of spans increases, the additional resonant modes

start to merge to create the familiar pass bands and stop bands. This is very well demonstrated in figures (15(c)) for a 50 span perfectly periodic beam.

#### 4.2 Periodic Beam on Flexible Supports

The above analysis was an extension of the results obtained for the L-shaped beam [3]. In that case, the number of resonant frequencies in each group of modes was two, corresponding to the two span, but as the number of spans increased, so did the number of resonant frequencies. Since the beam spans were on rigid supports, only one type of motion, rotational motion, at the support had to be considered. In the case of flexible supports, to which one may associate both stiffness, inertia or damping, both translational and rotational motions need to be considered at the junctions, and thus the number of mobility functions for each beam span will increase, apart from the introduction of additional mobility terms to describe the support in translation and in rotation.

Since mobility terms describe the support conditions, the end boundaries of the beams are free - free. Thus considering the two spans shown in figures (16), the mobility expressions are (assuming for support no coupling between translational and rotational motion):

$$\begin{aligned}
 V_1 &= F M_1 + F_A M_{12} + T_A Q_{12} \\
 V_A &= F M_{21} + F_A M_2 + T_A Q_2 \\
 &= -F_A M_{3T} - T_A Q_3 \\
 \theta_A &= F N_{21} + F_A N_2 + T_A L_2 \\
 &= -F_A N_3 - T_A L_{3T}
 \end{aligned}
 \tag{14}$$

where

$$M_{3T} = \left[ \frac{1}{M_3} + \frac{1}{M_s} \right]^{-1}$$

and

$$L_{3T} = \left[ \frac{1}{L_3} + \frac{1}{L_s} \right]^{-1}$$

M, N, L and Q in these expressions are used to defined the mobility



functions where  $M = V/F$  ;  $N = \dot{\theta}/F$  ;  $L = \dot{\theta}/T$  ;  $Q = V/T = \dot{\theta}/F$  . The single and double subscripts for  $M$ ,  $N$ ,  $L$  and  $Q$  represent input and transfer mobilities of the spans respectively, while  $M_s$  and  $L_s$  represent the mobilities of the support.  $F_i$  and  $T_i$  ( $i = A, B, \dots$ ) represent the input and junction forces and  $T_i$  ( $i = A, B, \dots$ ) represent the junction moment. At the junction, the mobility of the span end, and the mobility of the support would be in parallel since both have the same motion but share the force, and thus the total mobility is obtained using the reciprocal summation rule.

Extending the relationships of equation (14) to a four span periodic structure (figure 16) with flexible supports between the spans and at the ends, using the model in figure (16), the two matrix equations are one given by the product of the following matrix

$$\left[ \begin{array}{ccccc|ccc}
 (M_a + M_1) & -M_{12} & 0 & 0 & 0 & -Q_{12} & 0 & 0 \\
 -M_{21} & (M_2 + M_{3T}) & -M_{34} & 0 & 0 & (Q_2 + Q_3) & -Q_{34} & 0 \\
 0 & -M_{43} & (M_4 + M_{5T}) & -M_{56} & 0 & -Q_{43} & (Q_4 + Q_5) & -Q_{56} \\
 0 & 0 & -M_{65} & (M_6 + M_{7T}) & -M_{78} & 0 & -Q_{65} & (Q_6 + Q_7) \\
 0 & 0 & 0 & M_{87} & (M_8 + M_c) & 0 & 0 & -Q_{87} \\
 \hline
 -N_{21} & (N_2 + N_3) & -N_{34} & 0 & 0 & (L_2 + L_{3T}) & -L_{34} & 0 \\
 0 & -N_{43} & (N_4 + N_5) & -N_{56} & 0 & -L_{43} & (L_4 + L_{5T}) & -L_{56} \\
 0 & 0 & -N_{65} & (N_6 + N_7) & -N_{78} & 0 & -L_{65} & (L_6 + L_{7T})
 \end{array} \right] \quad (15a)$$

with the vector for the forces and moments;

$$\{ F_A, F_B, F_C, F_D, F_E, T_B, T_C, T_D \} \quad (15b)$$

and being equal to;

$$\{ -M_{1b} F, -M_{2b} F, 0, 0, 0, -N_{2b} F, 0, 0 \} \quad (15c)$$

and

$$\begin{bmatrix} v_b \\ v_A \\ v_B \\ v_C \\ v_D \\ v_E \\ \cdot \\ \theta_B \\ \cdot \\ \theta_C \\ \cdot \\ \theta_D \end{bmatrix} = \begin{bmatrix} M_b & M_{b1} & -M_{b2} & 0 & 0 & 0 \\ 0 & -M_a & 0 & 0 & 0 & 0 \\ 0 & 0 & M_{3T} & -M_{34} & 0 & 0 \\ 0 & 0 & 0 & M_{5T} & -M_{56} & 0 \\ 0 & 0 & 0 & 0 & -M_{7T} & -M_{78} \\ 0 & 0 & 0 & 0 & 0 & M_c \\ \hline 0 & 0 & N_3 & -N_{34} & 0 & 0 \\ 0 & 0 & 0 & N_5 & -N_{56} & 0 \\ 0 & 0 & 0 & 0 & N_7 & -N_{78} \end{bmatrix} \begin{bmatrix} -Q_{b2} & 0 & 0 \\ 0 & 0 & 0 \\ Q_3 & -Q_{34} & 0 \\ 0 & Q_5 & -Q_{56} \\ 0 & 0 & Q_7 \\ 0 & 0 & 0 \\ \hline L_{3T} & -L_{34} & 0 \\ 0 & L_{5T} & -L_{56} \\ 0 & 0 & L_{7T} \end{bmatrix} \begin{bmatrix} F \\ F_A \\ F_B \\ F_C \\ F_D \\ F_E \\ \cdot \\ T_B \\ \cdot \\ T_C \\ \cdot \\ T_D \end{bmatrix}$$

(16)

The solution of these matrix equations will give the power input and output for each element of the periodic structure. Results for the periodic beam on flexible supports using the above equations will be discussed in the next progress report.

### 5 CONCLUSIONS

In this progress report the modifications for the mobility power flow expressions to deal with two couple plate structures with different structural characteristics have been presented, together with a number of results for a parametric analysis that are compared to results obtained using an SEA approach. The results obtained using the mobility power flow approach represent details of the modal response both for the power input and power transferred curves as well as in the power ratio curves. Comparing these to the results obtained using an SEA approach, it can be observed that significant differences can be obtained between the actual results (represented by the mobility power flow results) and the mean level results obtained from an SEA analysis. These significant differences in the power ratio can be more pronounced in those cases where the response of

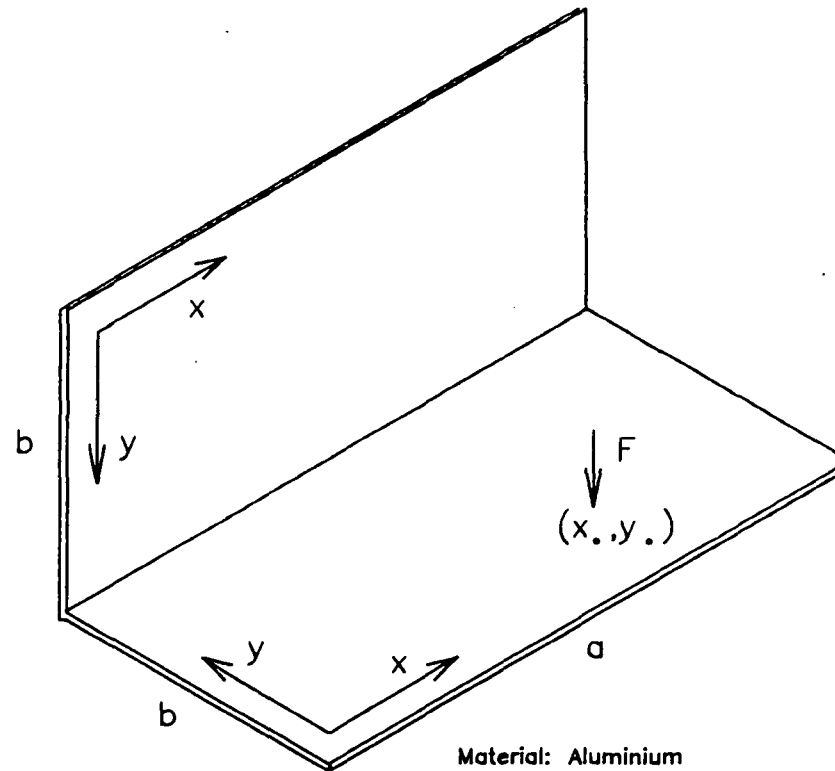
the global structure is dominated by modes of the receiver substructure. Under such conditions, while the general level of the power ratio may be low, at particular frequency, ratios close to unity can be obtained.

Also, presented in this report is a technique for applying the mobility power flow approach to the case of multi coupled structures. Matrix expressions and results are presented for a multiple span periodic beam with rigid supports and also the relevant expressions are derived for flexible supports. This analysis represents one application of the mobility power flow method which can be applied to both one dimensional and two dimensional junctions representing periodic beams and plates respectively.

In completing the analysis on the L-shaped plate, experimental measurements need to be performed to verify the analytical results. This will be the topic for the future work, after completing the analysis for distributed excitation on the source panel of the L-shaped plate. In performing this experimental analysis, it would be required that some development be achieved in measuring power flow near structural discontinuities without the use of a large number of transducers which would make the measurement cumbersome. This will be addressed in future work in this area.

#### REFERENCES

1. J. M. Cuschieri, "Parametric and Experimental Analysis Using a Power Flow Approach", Third semi-annual Report, Grant Number NAG-1-685, NASA Langley Research Center, Hampton, VA. (1988).
2. J. M. Cuschieri, "Extension of Vibrational Power Flow Techniques to Two-Dimensional Structures", Second Semi-annual Report, Grant Number NAG-1-685, NASA Langley Research Center, Hampton, VA. (1987).
3. J. M. Cuschieri, "Power Flow as a Complement to Statistical Energy Analysis and Finite Element Analysis", ASME Publication NCA - Vol 3 (1987).
4. R. J. Pinnington , R. G. White (1981) Journal of Sound and Vibration 75, 179-197, "Power Flow Through Machine Isolators to Resonant and Non-Resonant Beams.



Material: Aluminium  
Density: 2710 Kg/m<sup>3</sup>  
Elastic Modulus: 7.2 x10<sup>10</sup> N/m<sup>2</sup>  
Thickness: 0.00635m  
Dimensions: a=1.0m, b=0.5m  
Loss Factor: 0.01

Figure 1. Plate structure showing plate characteristics.

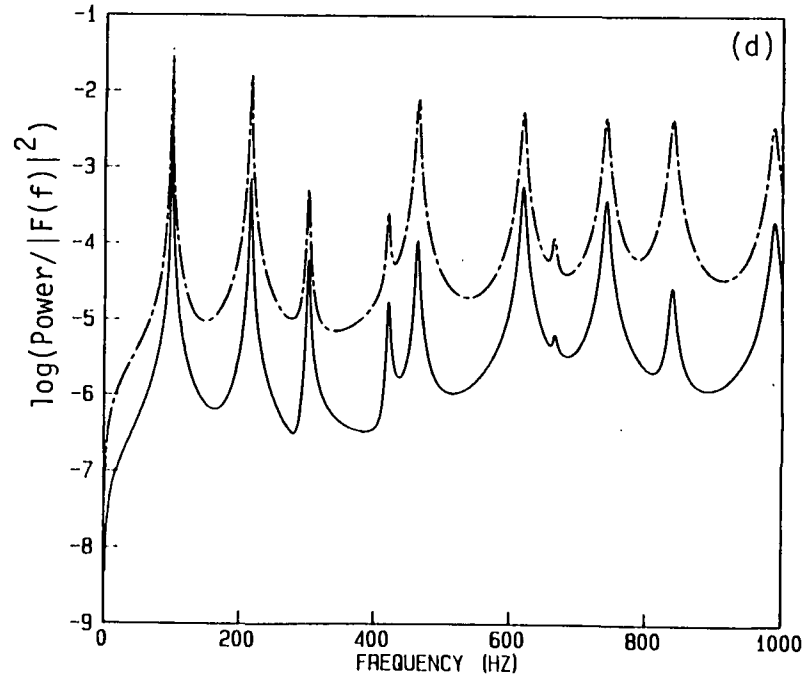
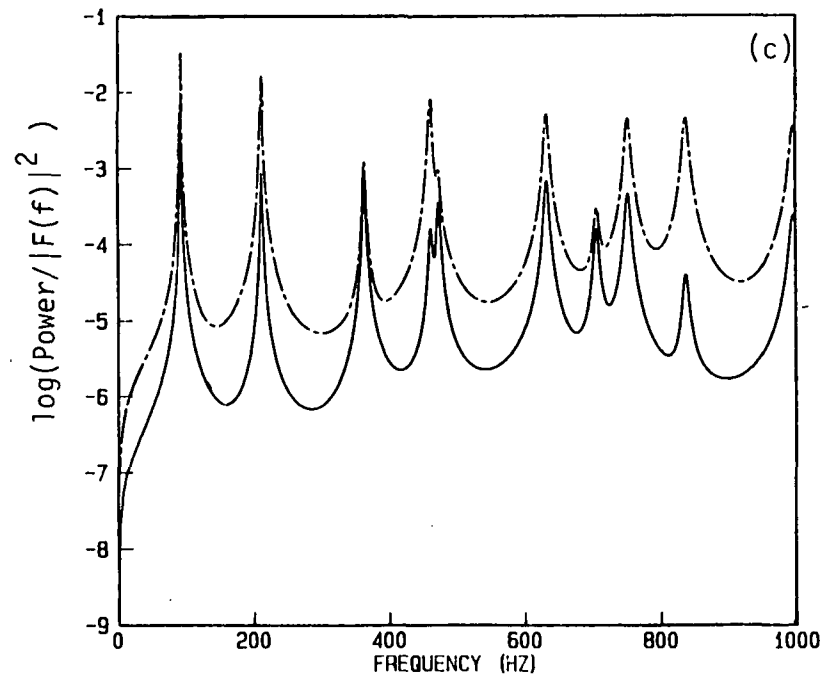
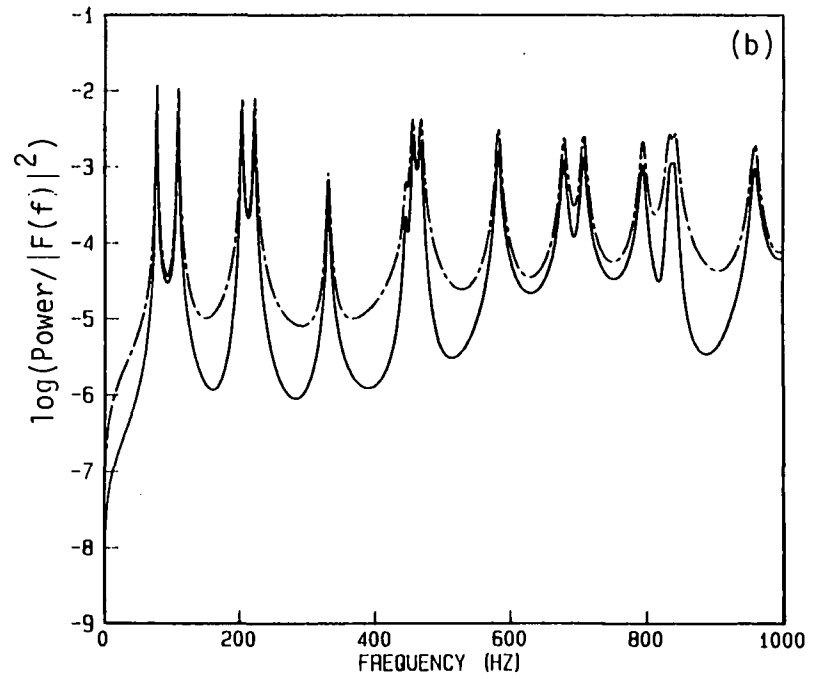
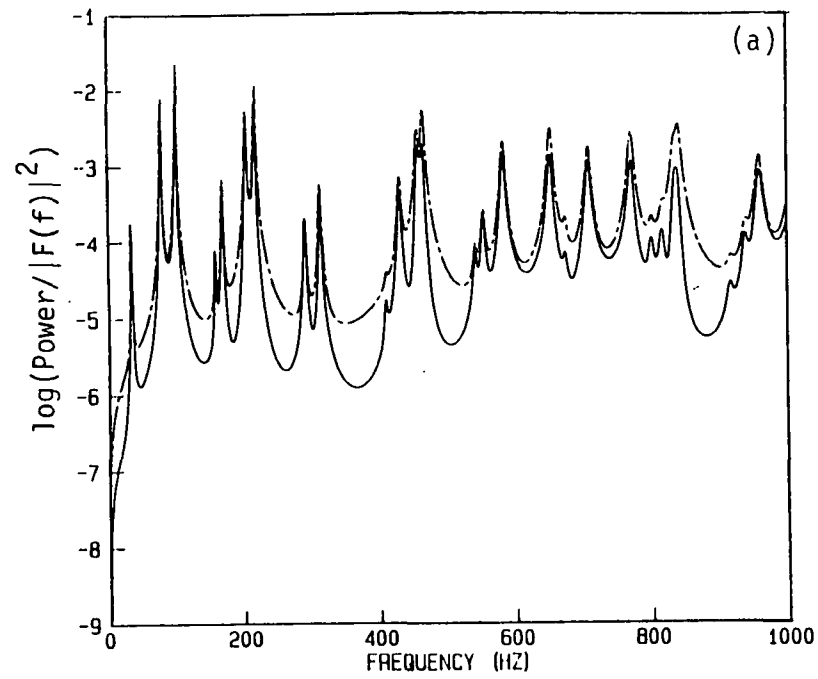


Figure 2. Power input and power transfer curves for different area ratios, using the mobility power flow,     :power transfer; -.-.-: power input. (a) 2.0; (b) 1.0; (c) 0.5; (d) 0.25 .

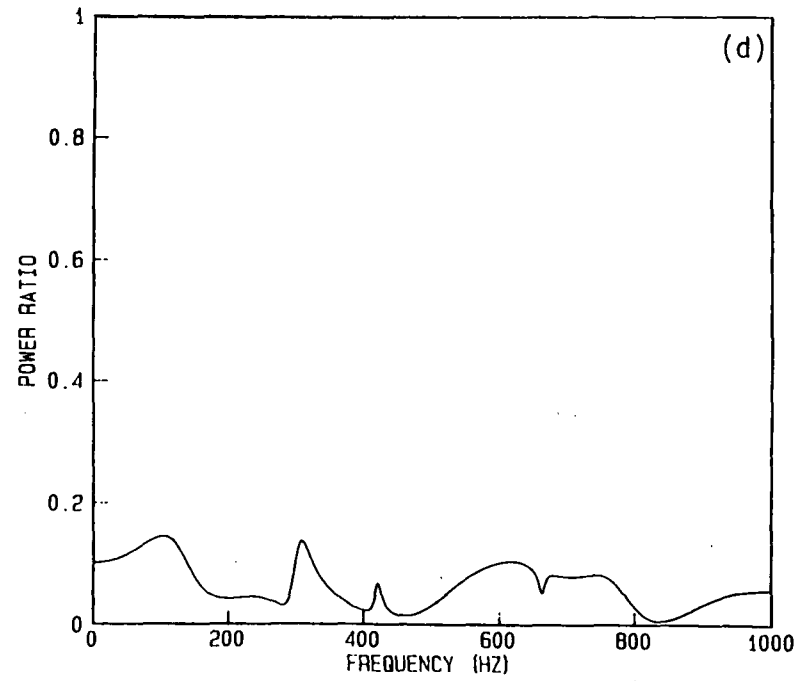
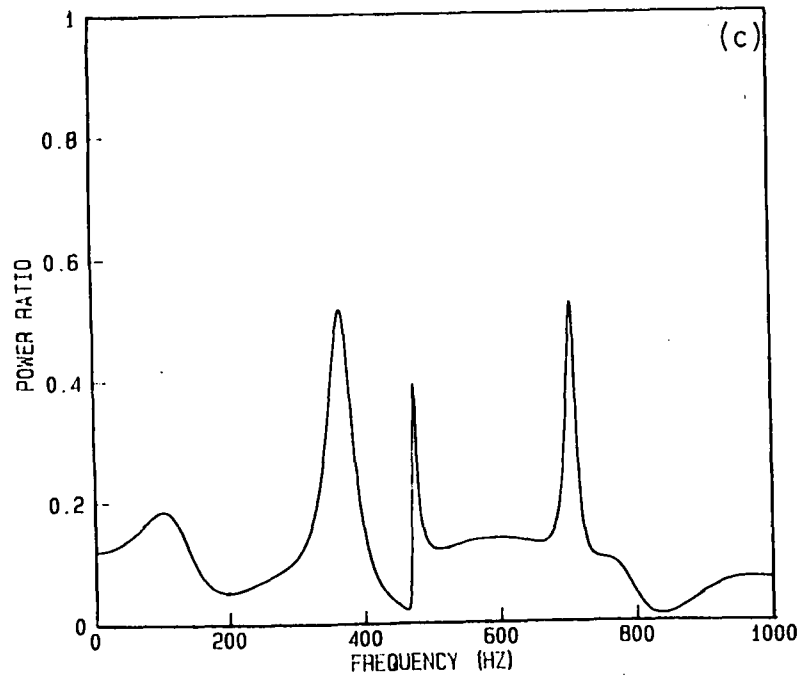
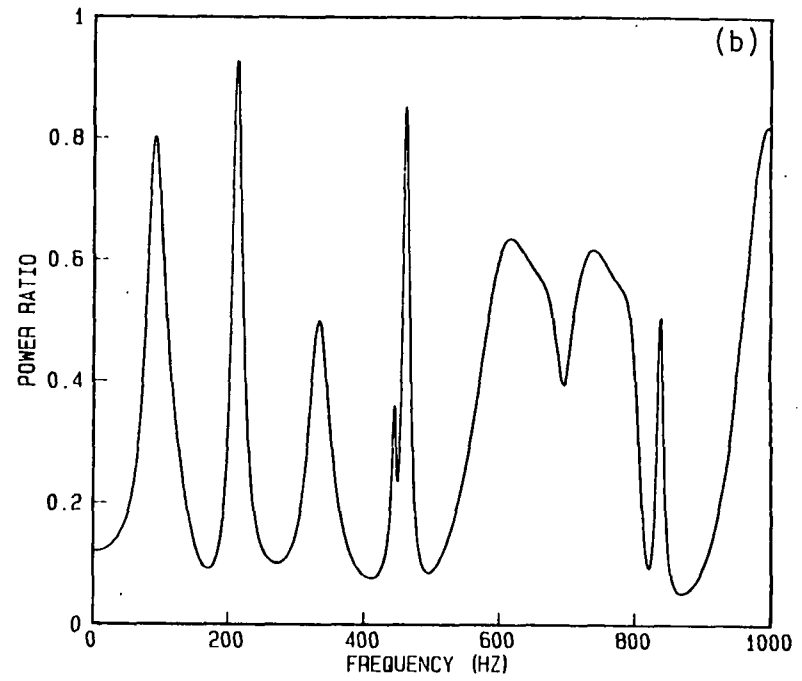
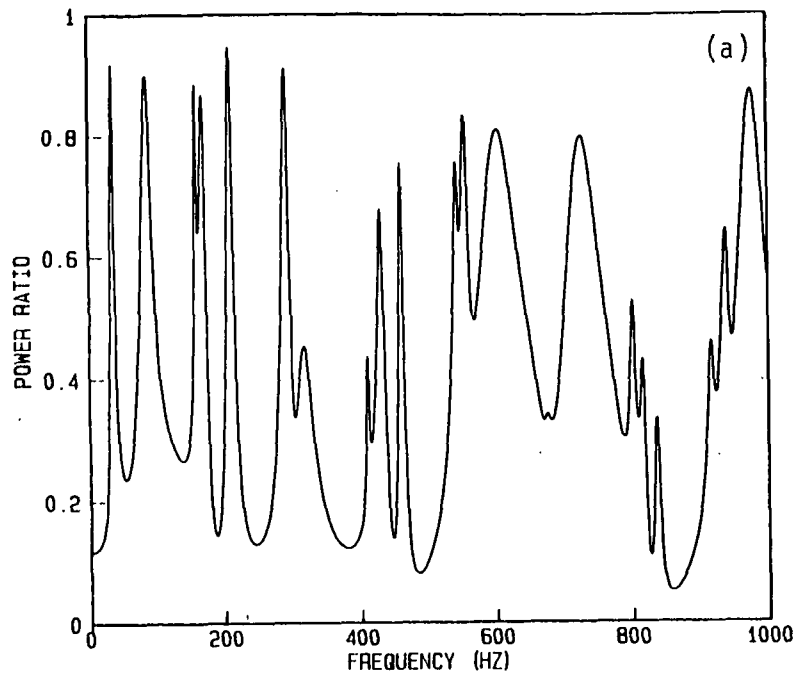


Figure 3. Power ratio curves for different area ratios, (a) 2.0; (b) 1.0; (c) 0.5; (d) 0.25 ..

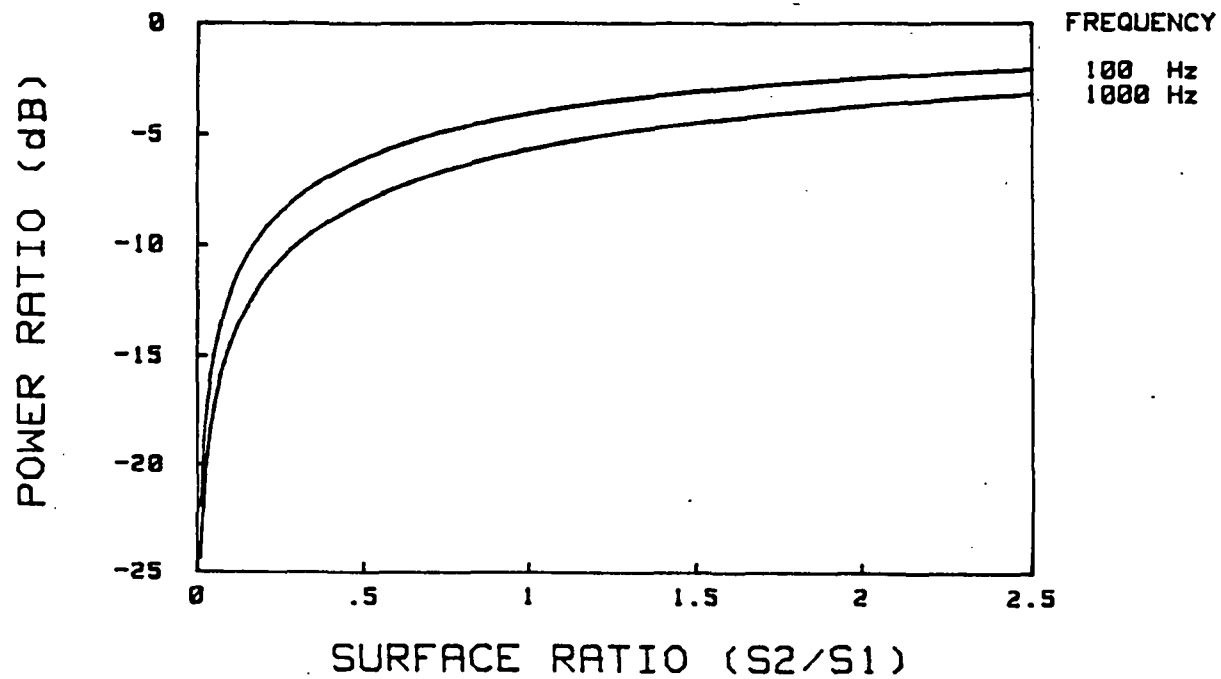


FIGURE 4. Power Ratio as a Function of the Area Ratio of the two plates using an SEA approach (reference 1).

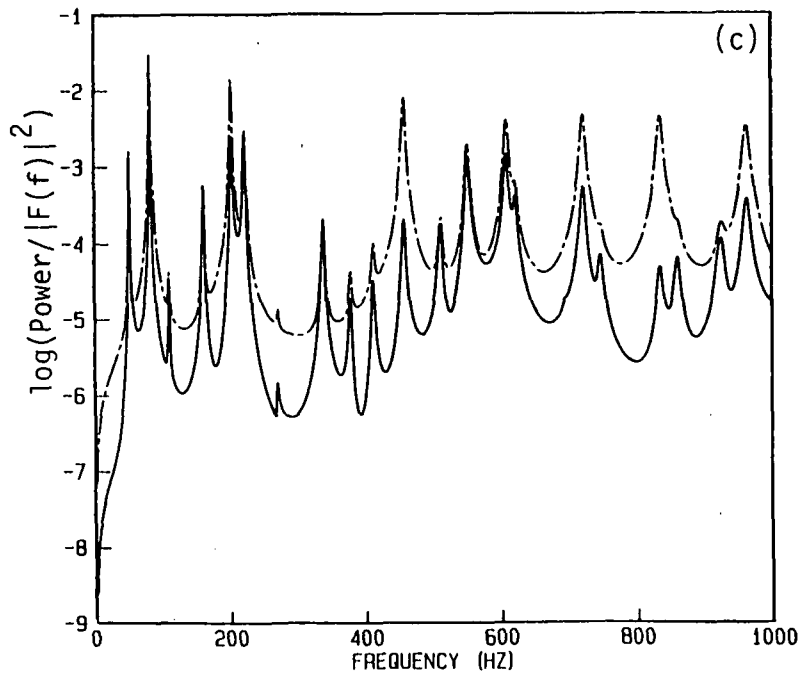
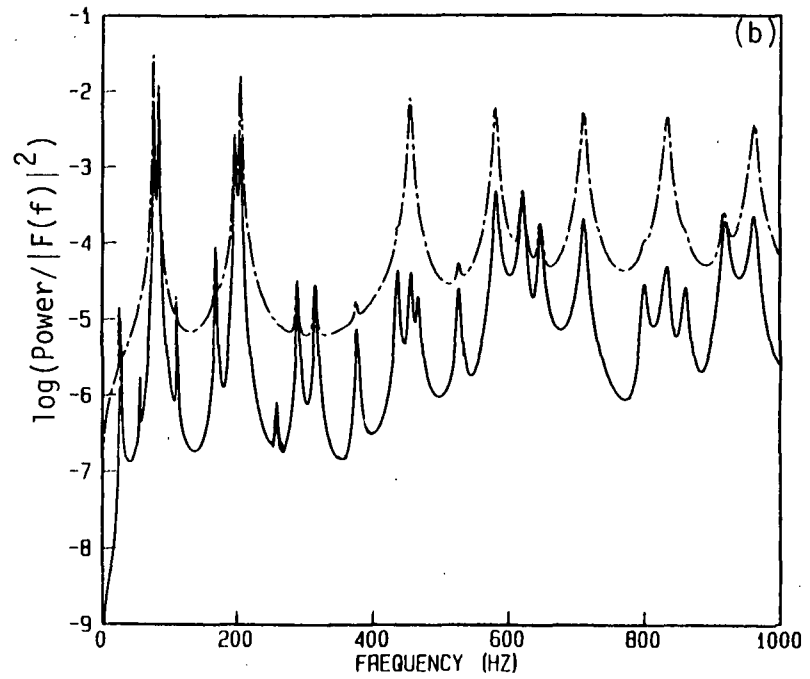
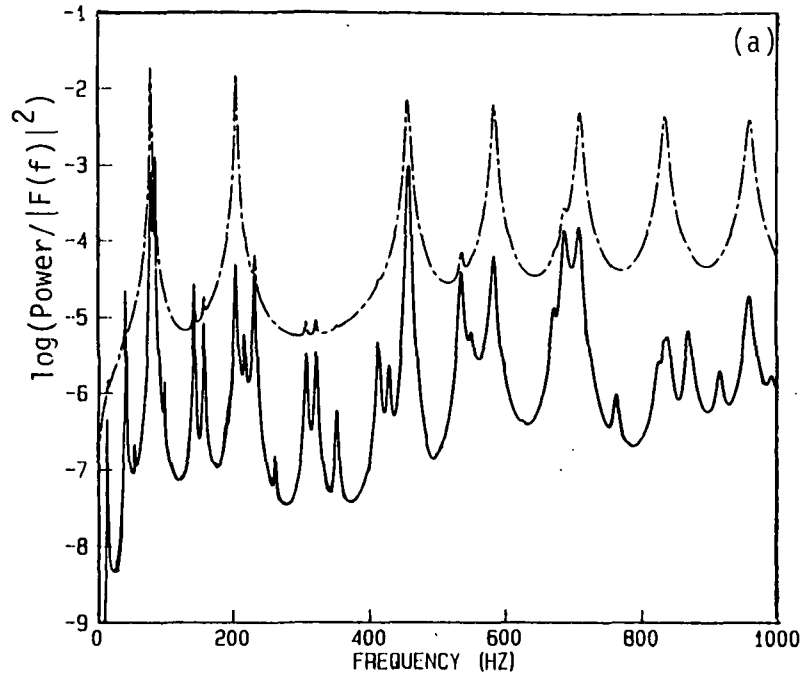


Figure 5. Continues on next page.



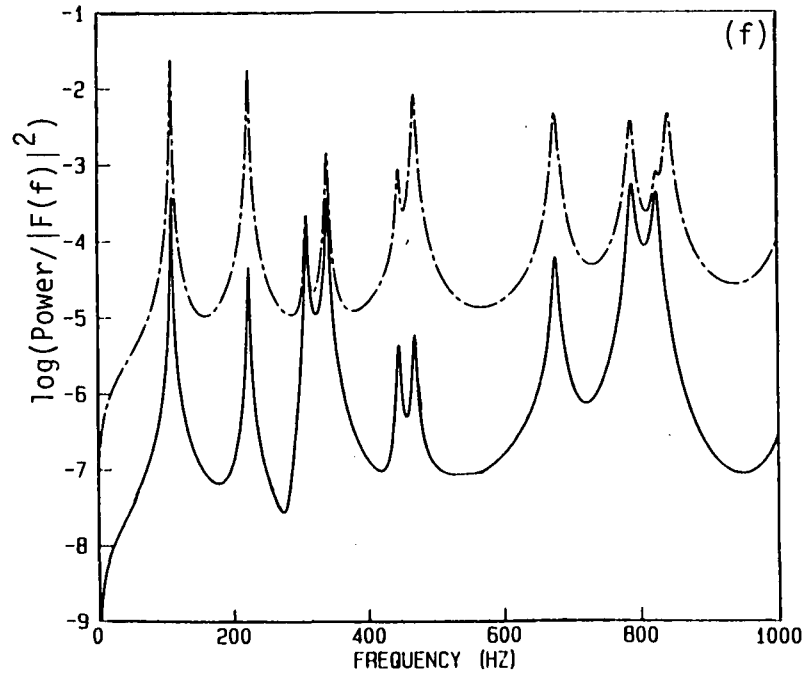
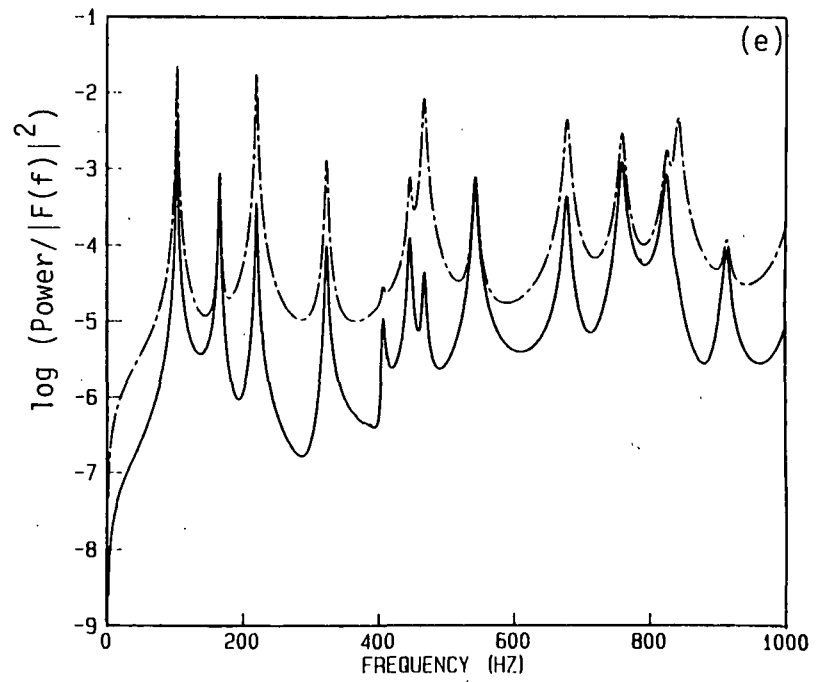
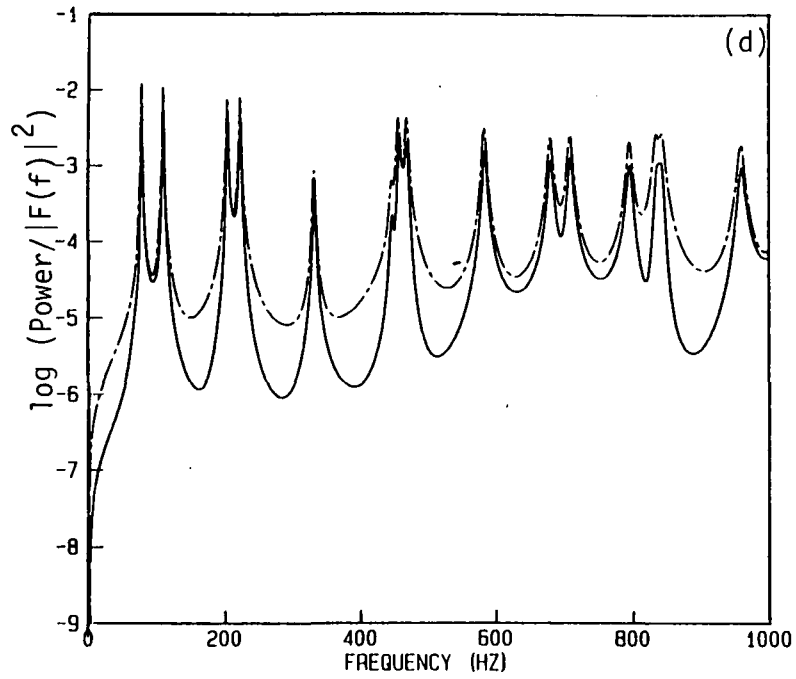


Figure 5. Mobility power flow results for the power input (---) and power transfer (\_\_\_) for different thickness ratios, (a) 0.125; (b) 0.25; (c) 0.5; (d) 1.0; (e) 2.0; (f) 4.0 .

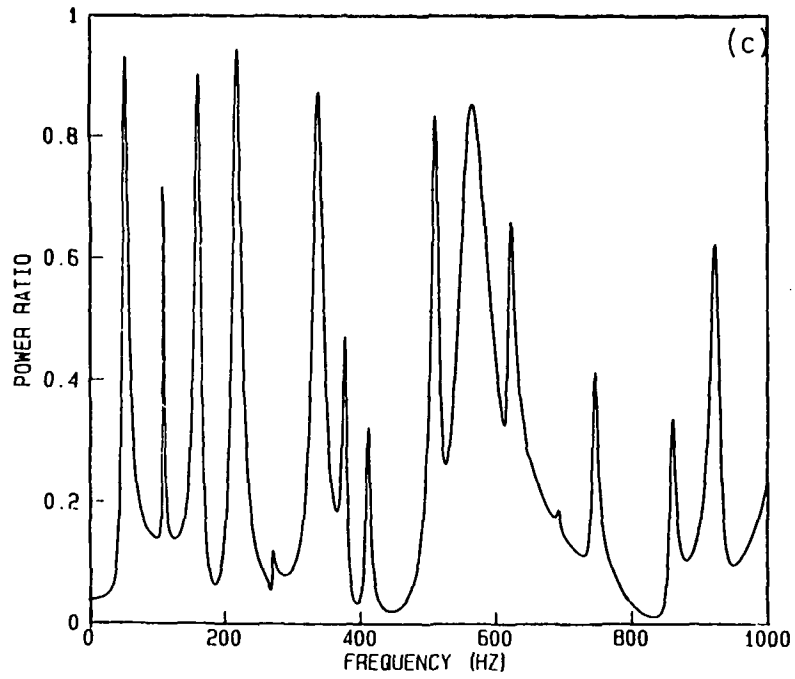
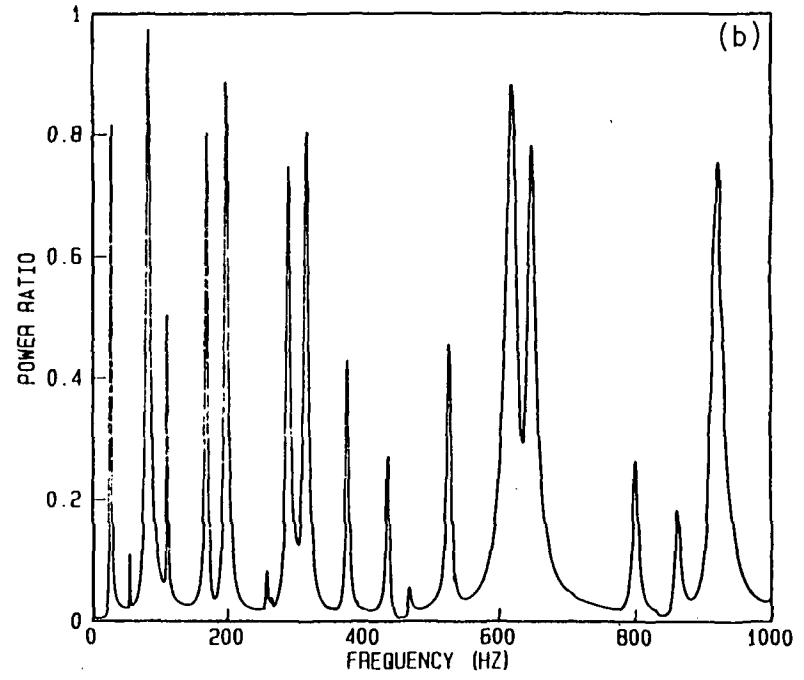
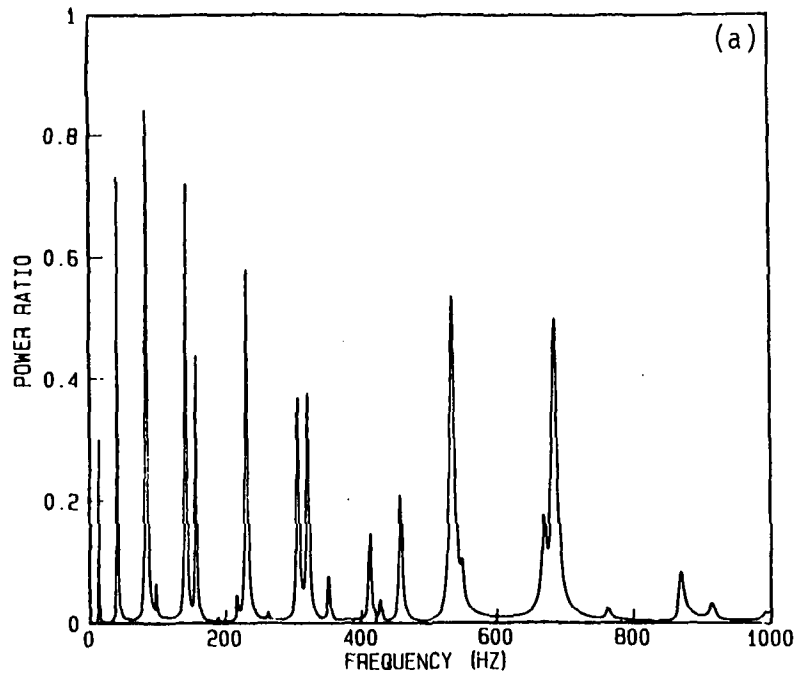


Figure 6. Continues on next page.

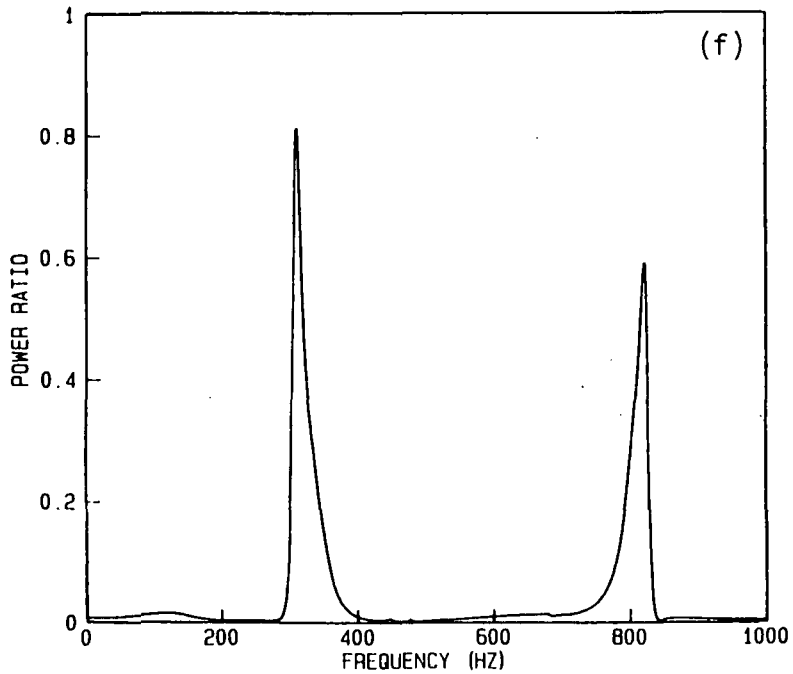
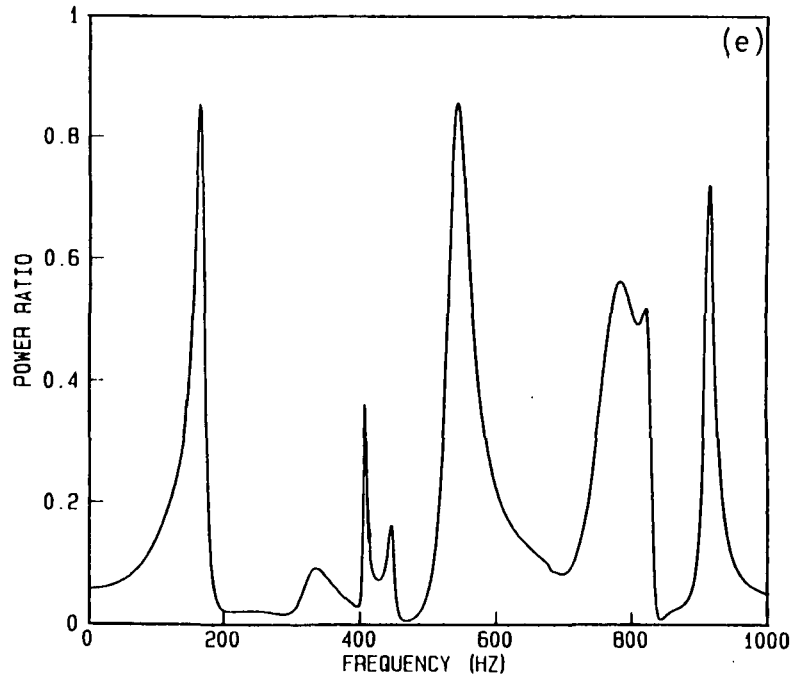
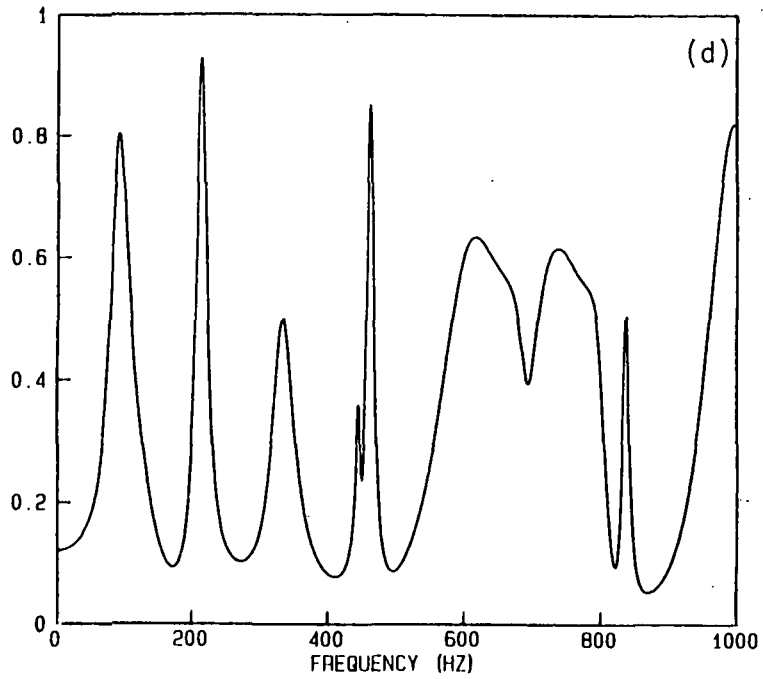


Figure 6. Power ratio results using the mobility power flow approach for different thickness ratios: (a) 0.125; (b) 0.25; (c) 0.5; (d) 1.0; (e) 2.0; (f) 4.0 .

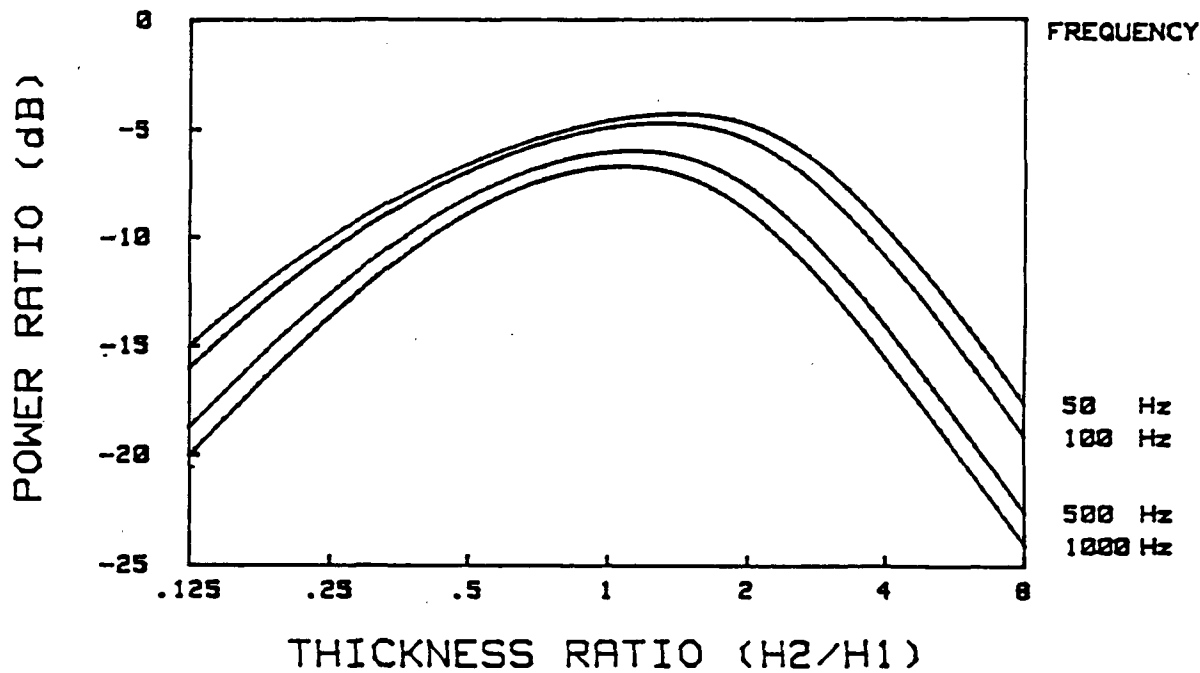


FIGURE 7. Power Ratio as a Function of the Thickness Ratio of two plates using SEA, (reference 1).

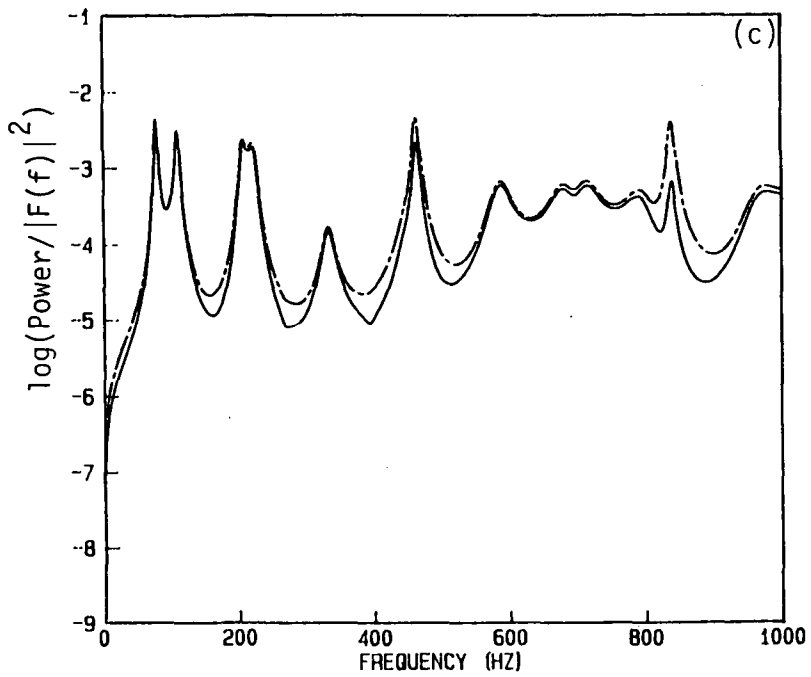
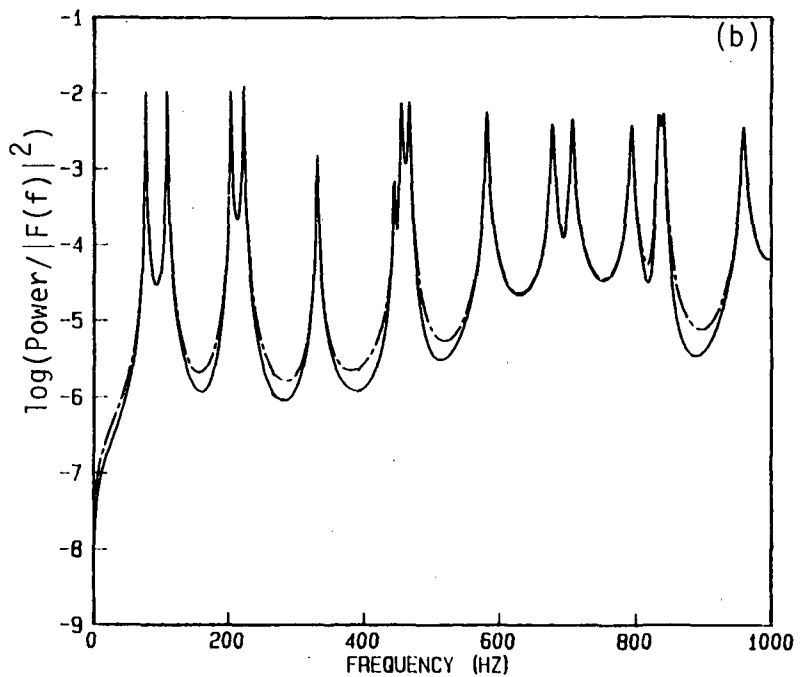
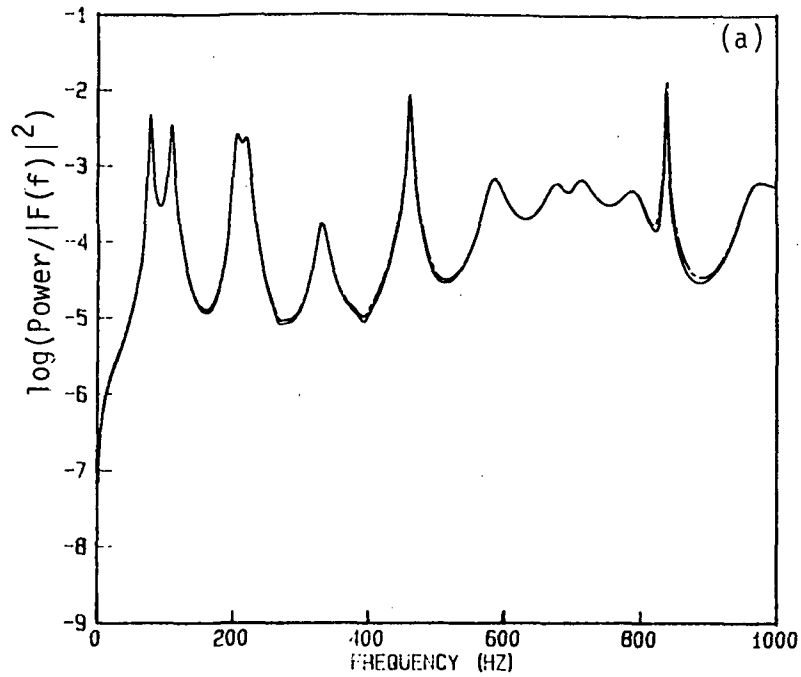


Figure 8. Continues on next page.

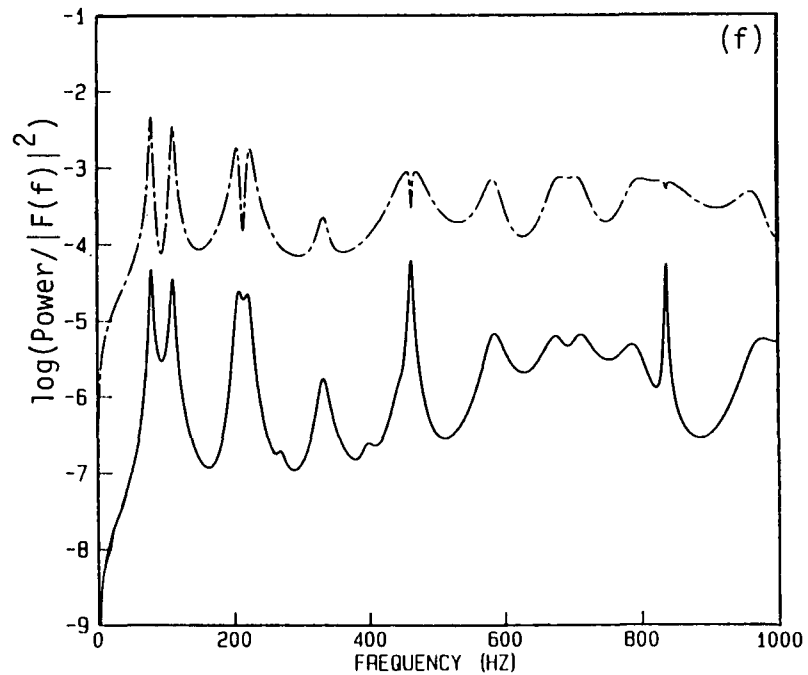
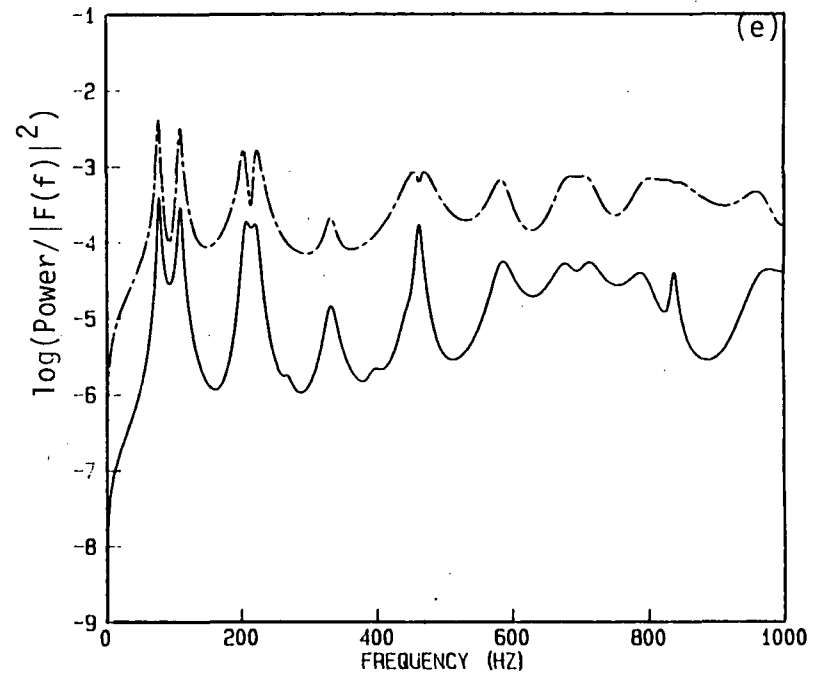
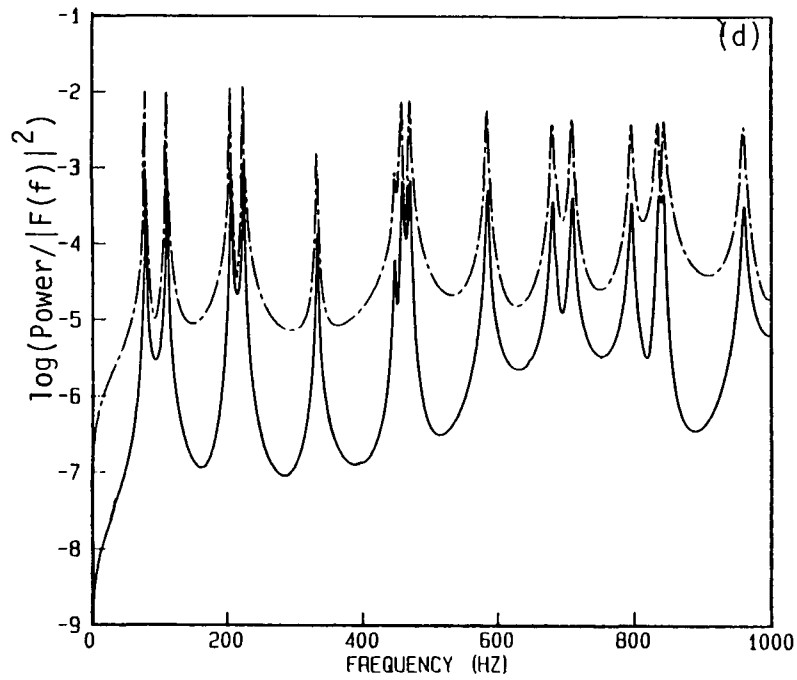


Figure 8. Power input (---) and power transfer (\_\_\_) results using a mobility power flow approach for different damping loss factor of source and receiver plates respectively. (a) 0.001/0.1; (b) 0.001/0.01; (c) 0.01/0.1; (d) 0.01/0.001; (e) 0.1/0.01; (f) 0.1/0.001 .

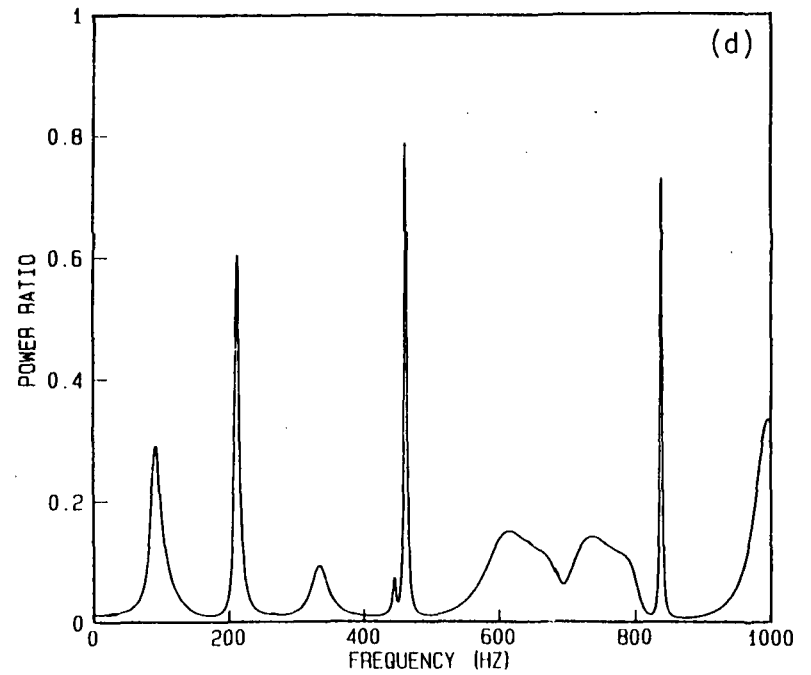
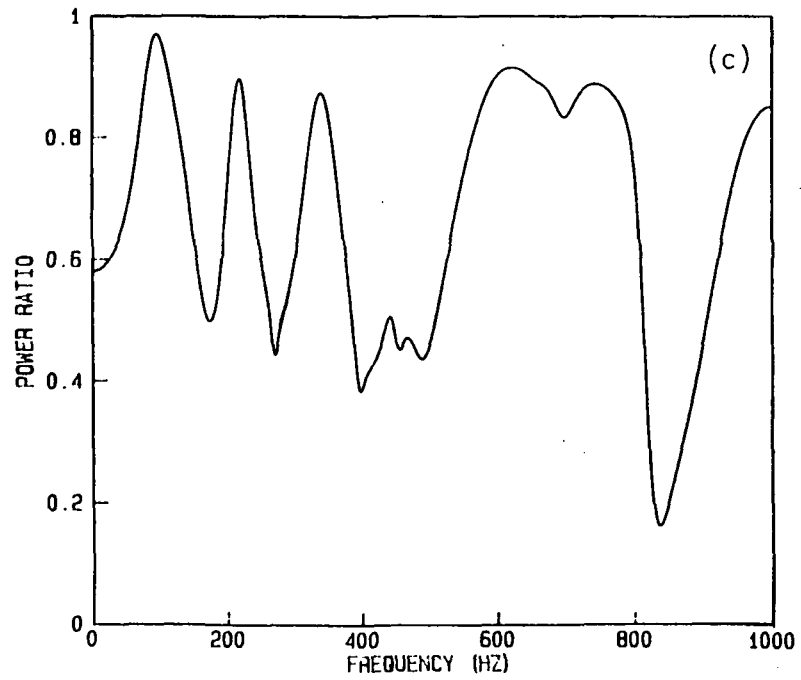
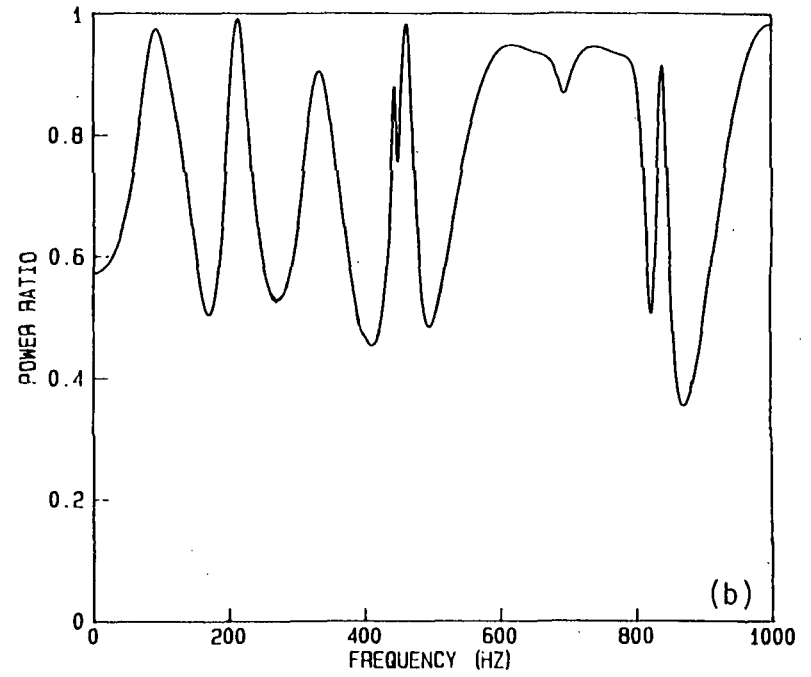
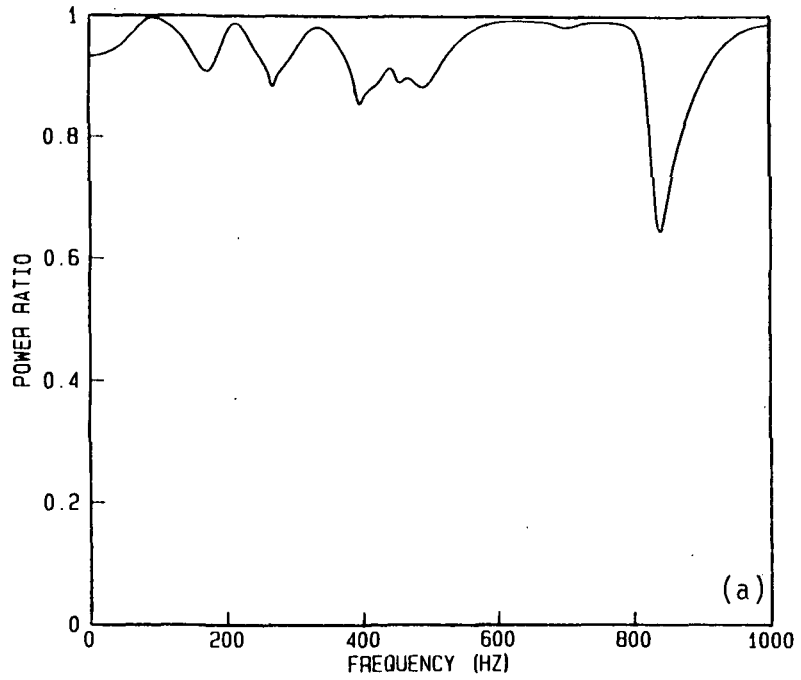


Figure 9. continues on next page.

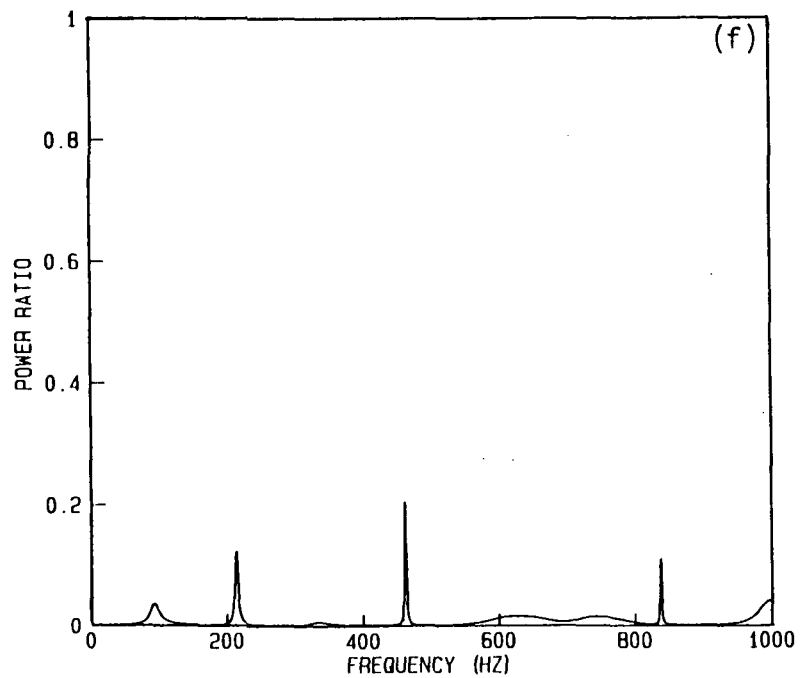
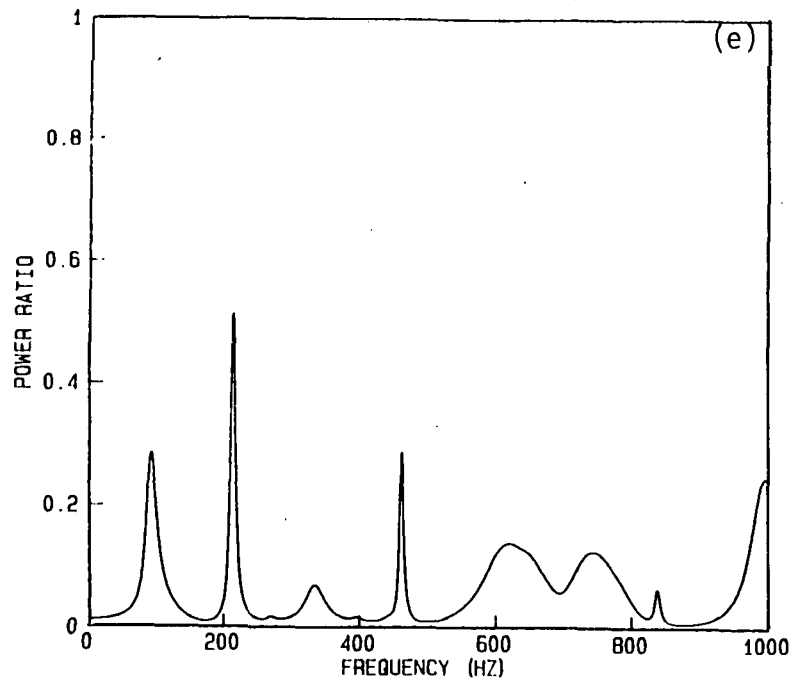


Figure 9. Power ratio results for different source and receiver plate damping loss factor.  
 (a) 0.001/0.1; (b) 0.001/0.01; (c) 0.01/0.1;  
 (d) 0.01/0.001; (e) 0.1/0.01; (f) 0.1/0.001 .

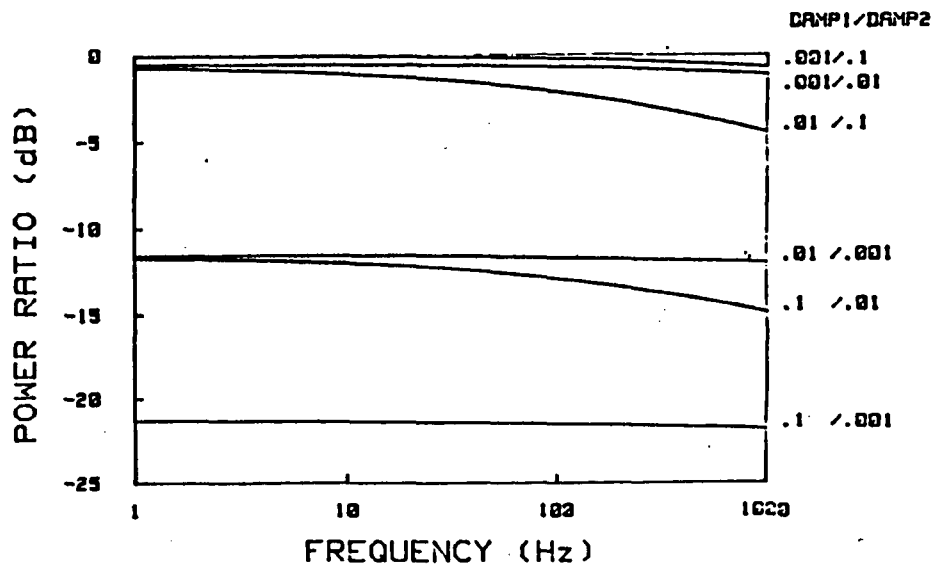


FIGURE 10. Power Ratio as a Function of Damping (plates with different damping).



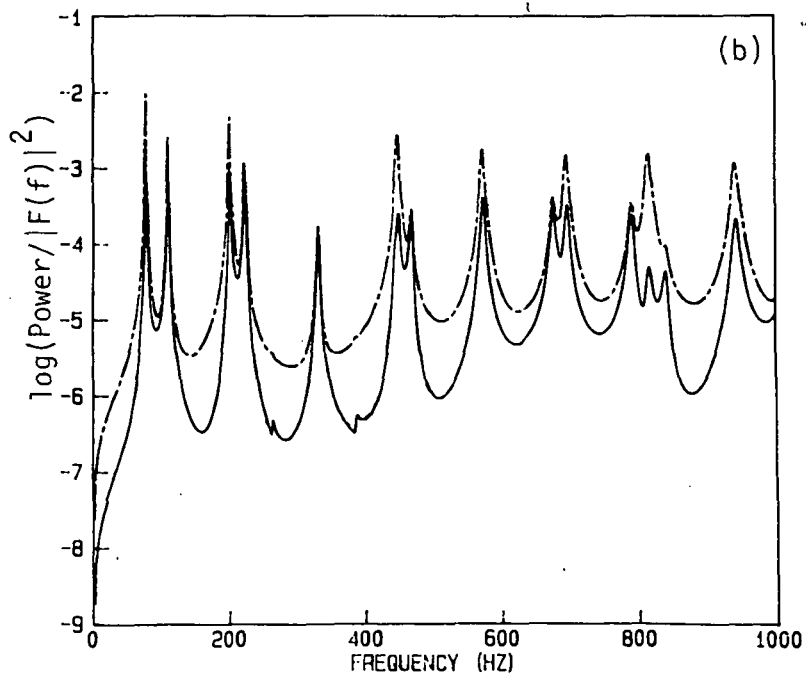
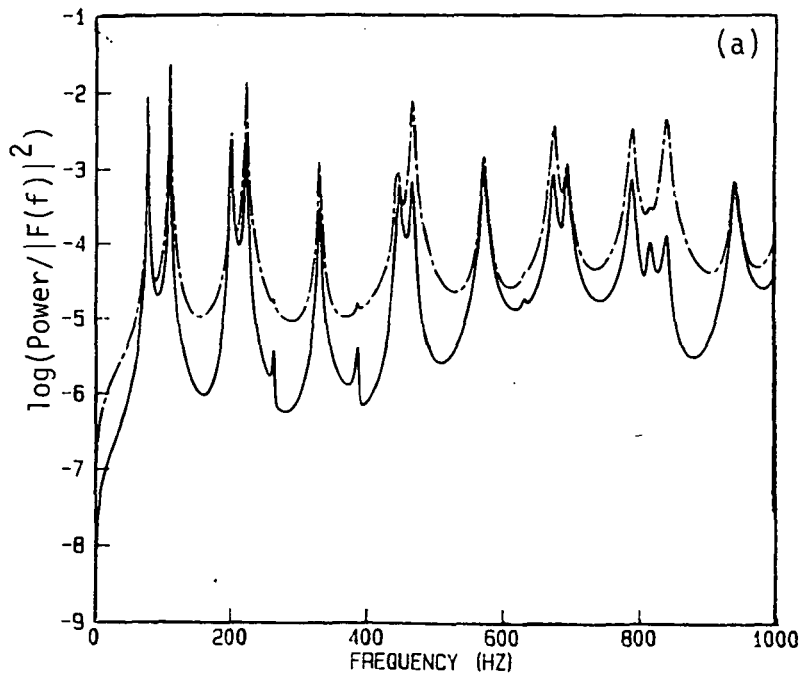


Figure 11. Power input (---) and power transfer (\_\_\_) results for different source plate and receiver plate materials. (a) Aluminium/steel; (b) steel/aluminium.

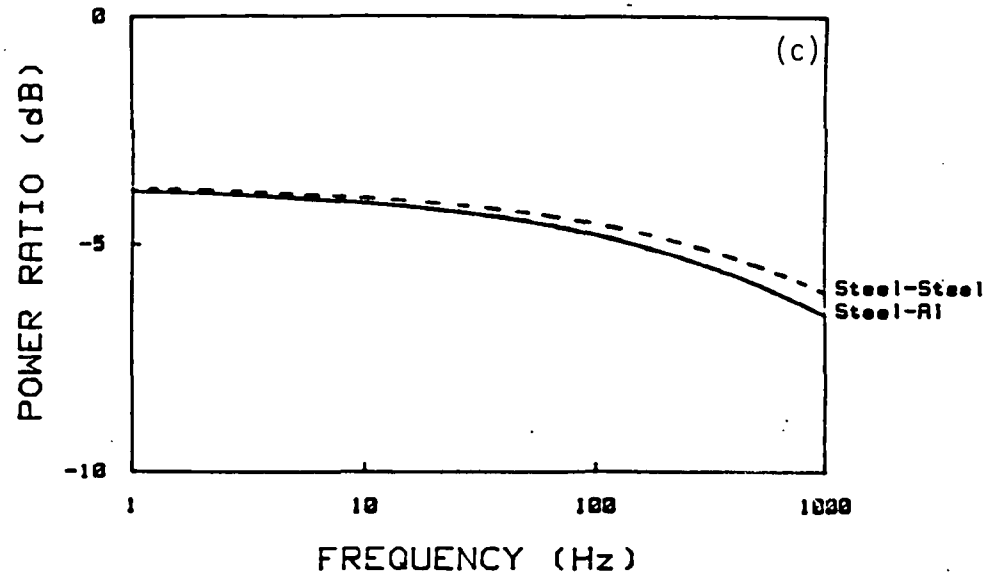
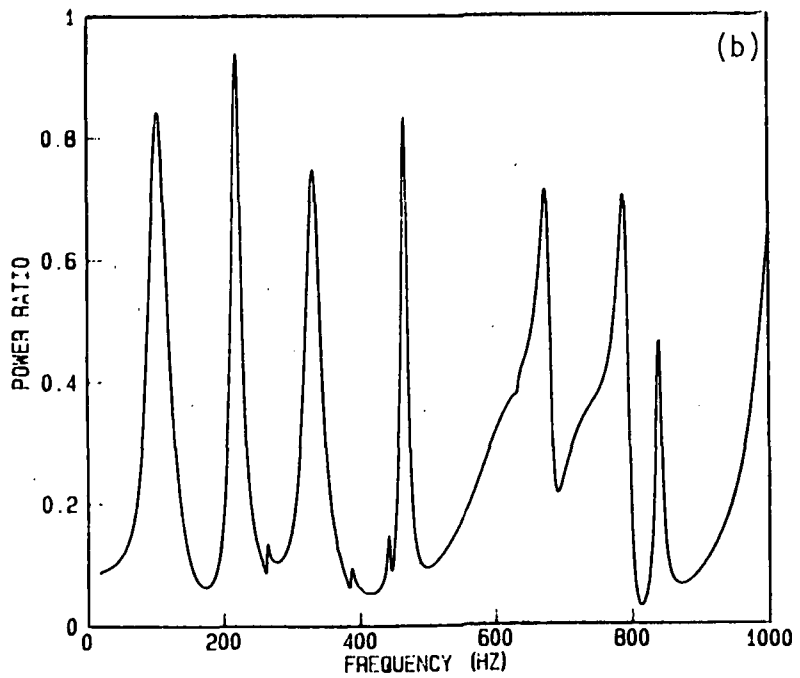
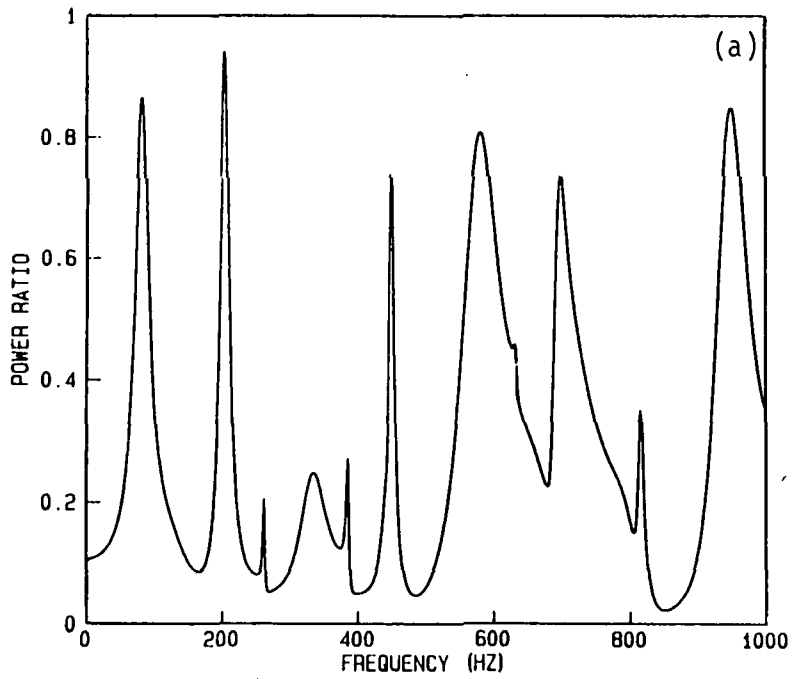


Figure 12. Power ratio for different materials, (a) Aluminium Steel; (b) steel/aluminium, both using mobility power flow approach; (c) SEA results.

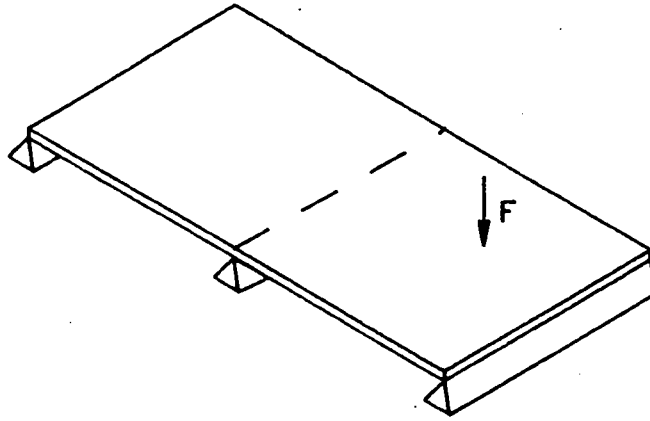


Figure 13. Alternative orientation for L-shaped plate for which the same results apply.

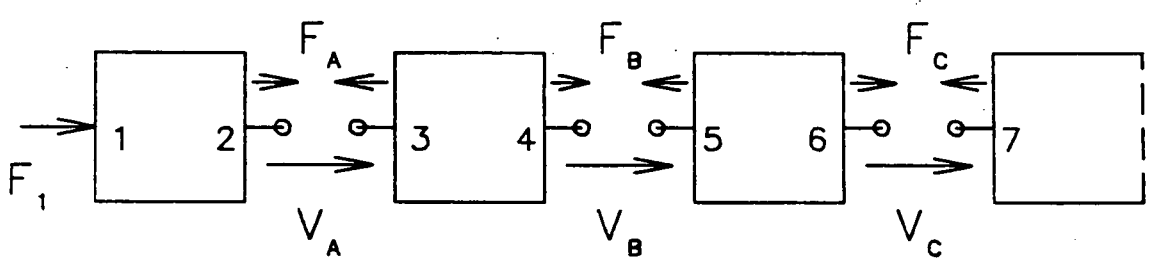


Figure 14. Model for coupled elements of a structure

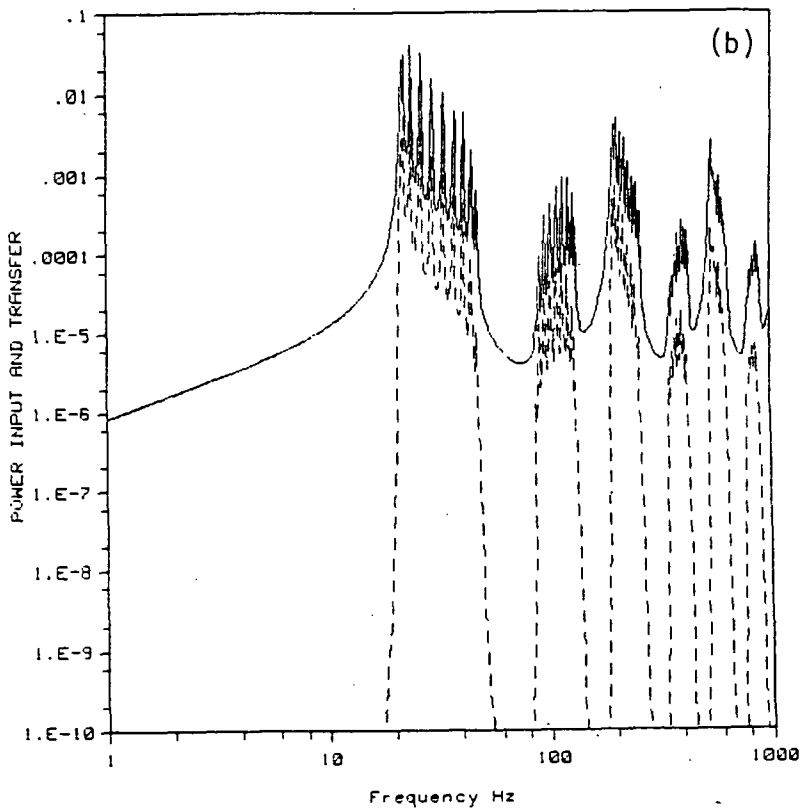
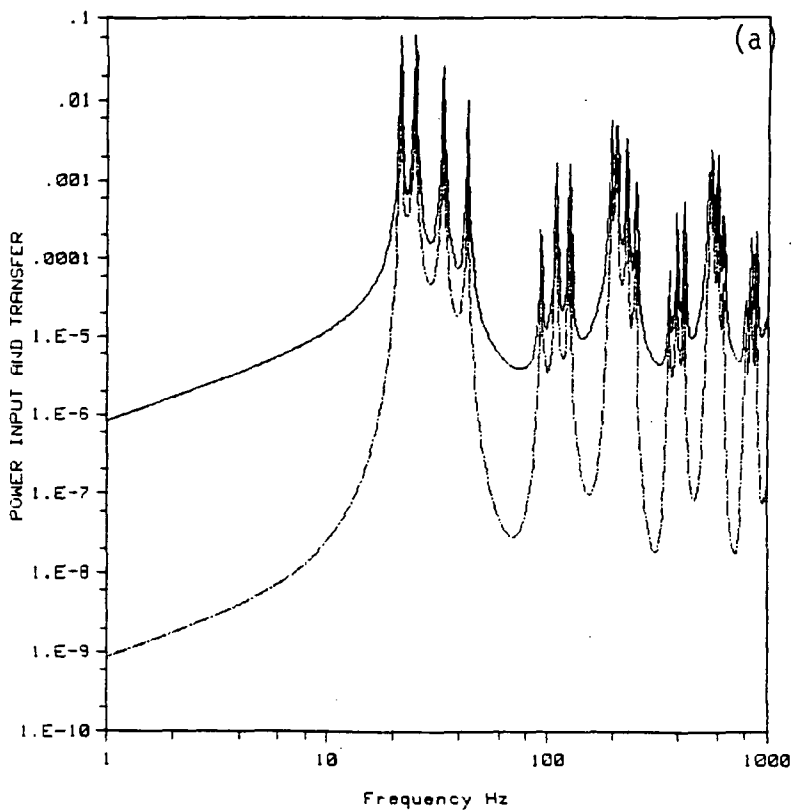


Figure 15 continues on next page.

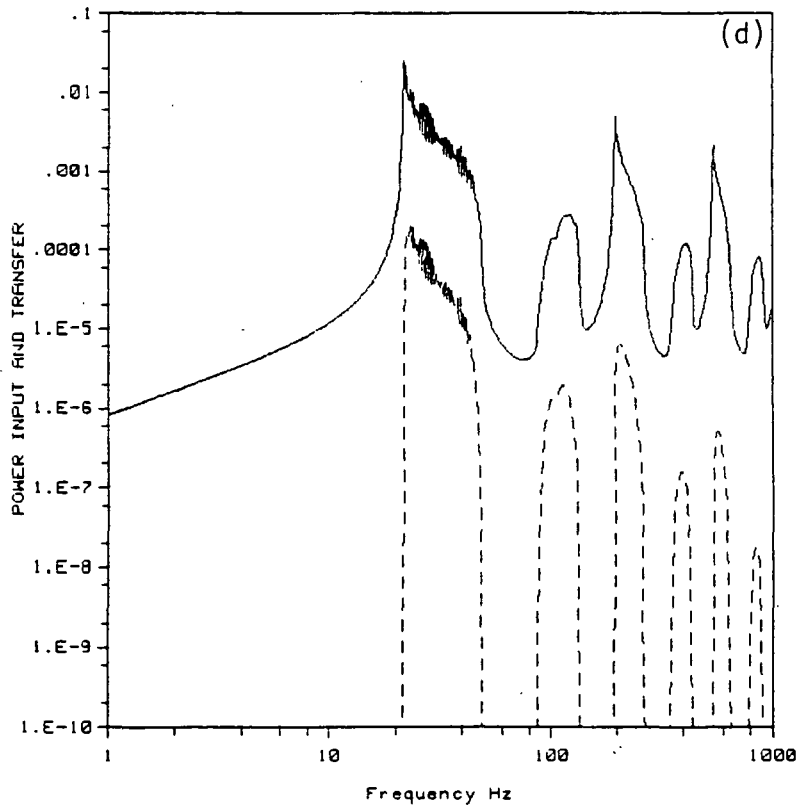
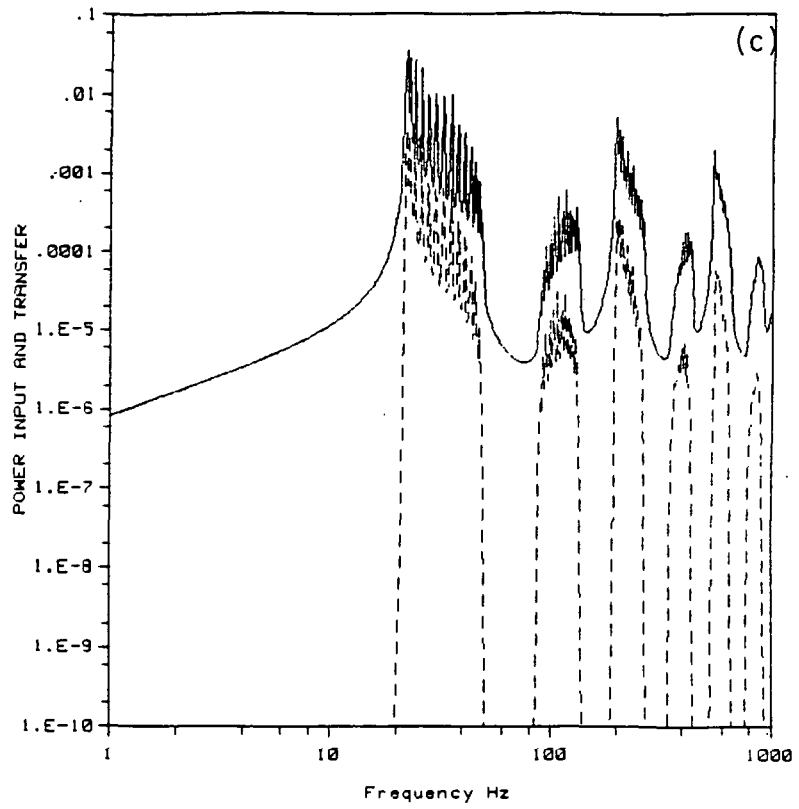


Figure 15. Power input and power transferred to last span per unit input load squared for a periodic beam on rigid supports. (a) 4 spans; (b) 10 spans; (c) 15 spans; (d) 50 spans.

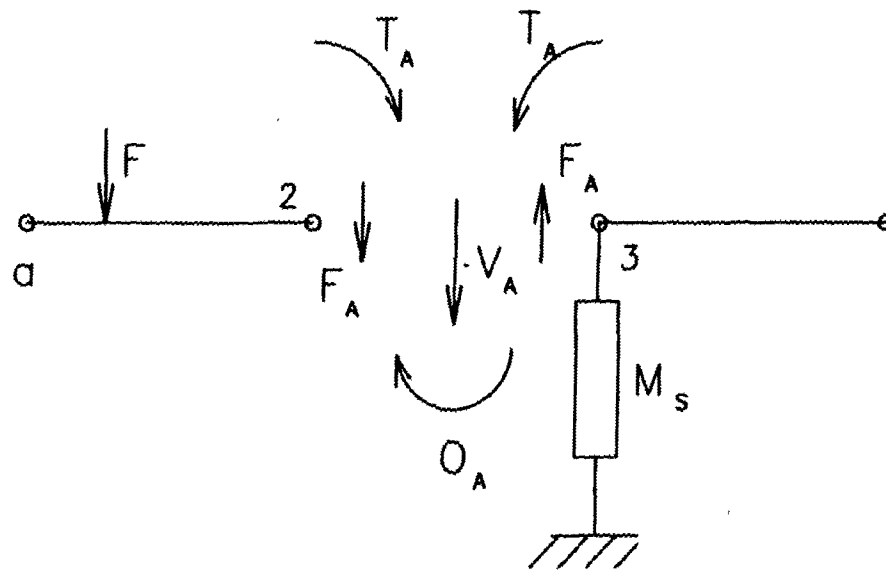


Figure 16. Model for periodic structure on flexible supports.